NAVAL POSTGRADUATE SCHOOL

MONTEREY, CALIFORNIA

THESIS

EXPERIMENTAL AND COMPUTATIONAL ANALYSIS OF A MINIATURE RAMJET AT MACH 4.0

by

Bryant R. Giorgi

September 2013

Thesis Advisor:	Garth V. Hobson
Second Reader:	Christopher M. Brophy

THIS PAGE INTENTIONALLY LEFT BLANK

REPORT DOCUMENTATION PAGE		Form Approved OMB No. 0704–0188

1. AGENCY USE ONLY *(Leave blank)*	2. REPORT DATE	3. REPORT TYPE AND DATES COVERED
	September 2013	Master's Thesis

4. TITLE AND SUBTITLE	5. FUNDING NUMBERS
EXPERIMENTAL AND COMPUTATIONAL ANALYSIS OF A MINIATURE RAMJET AT MACH 4.0	
6. AUTHOR(S) Bryant R. Giorgi	
7. PERFORMING ORGANIZATION NAME(S) AND ADDRESS(ES) Naval Postgraduate School Monterey, CA 93943–5000	**8. PERFORMING ORGANIZATION REPORT NUMBER**
9. SPONSORING/MONITORING AGENCY NAME(S) AND ADDRESS(ES) N/A	**10. SPONSORING/MONITORING AGENCY REPORT NUMBER**

11. SUPPLEMENTARY NOTES The views expressed in this thesis are those of the author and do not reflect the official policy or position of the Department of Defense or the U.S. Government. IRB Protocol number ____N/A____.

12a. DISTRIBUTION / AVAILABILITY STATEMENT	12b. DISTRIBUTION CODE
Approved for public release; distribution is unlimited.	A

13. ABSTRACT (maximum 200 words)

A miniature ramjet engine designed to perform at Mach 4.0 was tested in a supersonic wind tunnel. Cryogenic strain gauges were used to measure drag and Schlieren imaging techniques were used to observe the inlet Mach cone profile at Mach numbers of 4.0. Three different nozzle configurations were tested to confirm computational models used to predict back pressure and normal shock locations at the inlet.

Using ANSYS-CFX, a cold flow, computational fluid dynamics model of the ramjet in the wind tunnel was evaluated to compare with the experimental results. This model was then used as a base for an eddy dissipation combustion model. Hydrogen was modeled as being injected into the combustion chamber of the ramjet through inlet struts and then reacting with atmospheric oxygen to produce combustion. Drag predictions were inconclusive, however, the computational model remained stable during combustion calculations.

14. SUBJECT TERMS	15. NUMBER OF PAGES
Mach 4, Ramjet, Drag, Turbulence Modeling, Simulation, ANSYS CFX	92
	16. PRICE CODE

17. SECURITY CLASSIFICATION OF REPORT	18. SECURITY CLASSIFICATION OF THIS PAGE	19. SECURITY CLASSIFICATION OF ABSTRACT	20. LIMITATION OF ABSTRACT
Unclassified	Unclassified	Unclassified	UU

NSN 7540–01–280–5500 Standard Form 298 (Rev. 2–89)
Prescribed by ANSI Std. 239–18

THIS PAGE INTENTIONALLY LEFT BLANK

Approved for public release; distribution is unlimited

EXPERIMENTAL AND COMPUTATIONAL ANALYSIS OF A MINIATURE RAMJET AT MACH 4.0

Bryant R. Giorgi
Ensign, Unites States Navy
B.S., United States Naval Academy, 2012

Submitted in partial fulfillment of the
requirements for the degree of

MASTER OF SCIENCE IN MECHANICAL ENGINEERING

from the

NAVAL POSTGRADUATE SCHOOL
September 2013

Author: Bryant R. Giorgi

Approved by: Garth V. Hobson
Thesis Advisor

Christopher M. Brophy
Second Reader

Knox T. Millsaps
Chair, Department of Mechanical and Aerospace Engineering

THIS PAGE INTENTIONALLY LEFT BLANK

ABSTRACT

A miniature ramjet engine designed to perform at Mach 4.0 was tested in a supersonic wind tunnel. Cryogenic strain gauges were used to measure drag and Schlieren imaging techniques were used to observe the inlet Mach cone profile at Mach numbers of 4.0. Three different nozzle configurations were tested to confirm computational models used to predict back pressure and normal shock locations at the inlet.

Using ANSYS-CFX, a cold flow, computational fluid dynamics model of the ramjet in the wind tunnel was evaluated to compare with the experimental results. This model was then used as a base for an eddy dissipation combustion model. Hydrogen was modeled as being injected into the combustion chamber of the ramjet through inlet struts and then reacting with atmospheric oxygen to produce combustion. Drag predictions were inconclusive, however, the computational model remained stable during combustion calculations.

THIS PAGE INTENTIONALLY LEFT BLANK

TABLE OF CONTENTS

LIST OF FIGURES

LIST OF TABLES

THIS PAGE INTENTIONALLY LEFT BLANK

ACKNOWLEDGMENTS

I would like to take this space to thank my thesis advisor, Professor Garth Hobson, for his help, advice, and patience. Another huge piece of appreciation should be given to Mr. John Gibson for all the immense help he has given to keeping everything working here at the Turbopropulsion Lab, from the supersonic wind tunnel operations to the tedious and ever-present mandatory software updates these computers need. Thank you.

THIS PAGE INTENTIONALLY LEFT BLANK

I. INTRODUCTION

The idea of rotorless, air-breathing engine dates back to a French inventor named René Lorin. His idea was well before his time, however, as even he recognized that the velocities required to make the compression cycle of his engine work were in excess of the speed of sound in air. This was just not possible of aircraft before the First World War

The use of ramjets in military aircraft and weapons was intermittent after the second World War, with the most well-known example being Lockheed Martin's SR-71 Blackbird using the Pratt & Whitney J58 turbojet-assisted ramjets at unclassified speeds reaching Mach 3.2 at altitude. Ramjet application in both the military and civilian sectors waned after the retirement of the SR-71 platform in favor of more efficient (turbofan) and faster (SCRamjet) engines. However, a recent resurgence has been seen in the interest of the use of ramjets in military technology. November of 2006 saw the implementation of the BrahMos, the world's fastest cruise missile, into the arsenals of the Indian and Russian Federation's militaries. Interest in ramjets is currently spiking due to the design's potential to be scaled down because of the design's absence of moving integral parts. As the ranges demanded of certain weapons increase and the size of unmanned aerial systems decrease, ramjets are being looked at as the propulsion design of choice.

This thesis continues the work of Kevin M. Fergurson [1], Wee T. Khoo [2], and Bingqiang Chen [3] to analyze the performance envelope of a ramjet small enough to be ballistically launched from within a 35 mm diameter barrel.

In [1], a ramjet was designed for operation in a free stream velocity of Mach 4.0 and was then tested at operating speed in a supersonic wind tunnel (SSWT). Analyses were also done using the GRIDGEN and OVERFLOW computer programs for computational fluid dynamics (CFD). A follow-up was conducted in [2] with an attempt at using the CFD-FASTRAN code to model the combustion process in the ramjet. Unfortunately, the computing limitations and the two-dimensional model used prevented an optimal analysis of the operating conditions of the ramjet.

In [3], combustion CFD analysis was done using ANSYS-CFX with better but still sub-optimal results. An attempt to measure drag was also done in the SSWT using cryogenic strain gauges. For reasons that will be explained in Chapter III, the results of those drag measurements were not satisfactory. The ANSYS software did allow detailed, accurate cold-flow analyses of Mach 4.0 flow over the ramjet. These analyses revealed that the inlet conditions were not optimal. Thus, CFD analysis was done altering the nozzle by reducing the throat area of the converging-diverging section.

The present study seeks to refine the tests and data gathered from these preceding studies by continuing the CFD combustion analyses done in [3] and completely redesigning the drag measurement flexure arms, which hold the ramjet in the SSWT. The changes made were done in order to improve the quality of the data collected in the SSWT experimental drag measurement and the cold flow CFD drag prediction. To validate the CFD predictions done in [3] of the different nozzles, two of the nozzle designs with reduced throat areas were also tested in the SSWT with drag measurements recorded.

The data acquisition for the strain measurements was also upgraded to a National Instruments unit that was more user friendly. Additionally, the calibration procedure before and after testing of the ramjet in the SSWT was updated, which resulted in reduced uncertainty of the drag measurements.

II. SUPERSONIC WIND-TUNNEL EXPERIMENT

A. BACKGROUND AND METHODOLOGY

This experiment was run in [1], [2], and [3], and involves placing a model of the ramjet in the SSWT at the design speed of Mach 4.0. Drag was measured using strain gauges on the flexure arms of the holding struts.

In the SSWT experiment run in [1], imperfections in the model used in the wind tunnel resulted in an axisymmetric conical shock attached to the front of the nosecone. In [2], the strain gauges used were tested outside their normal temperature range, with the static temperature of the SSWT test section at 68 K. In [3], the instruments were able to take readings, but when the free stream velocity returned to zero, the readings failed to return to zero strain.

Thus, the goals for these rounds of experiments were:

- Run the model at Mach 4.0 and develop an axisymmetric, conical shock at the front of the nosecone.
- Account for changes in performance of gauges at low temperatures.
- Have the strain readings return to zero after the free stream returned to zero velocity.

B. EXPERIMENTAL SETUP

1. New Strut Design

In references [1], [2], and [3], two struts were used that attached to the ramjet in two locations, each with a pin in the front and a screw in the aft of the ramjet. For these experiments, to try and compensate for changes that may be due to thermal expansion, only one strut was used. This required some modification to replace the front pin attachment with a front attachment bolt (Figure 1) in order to make the structure more stable in the presence of flow reaching Mach four.

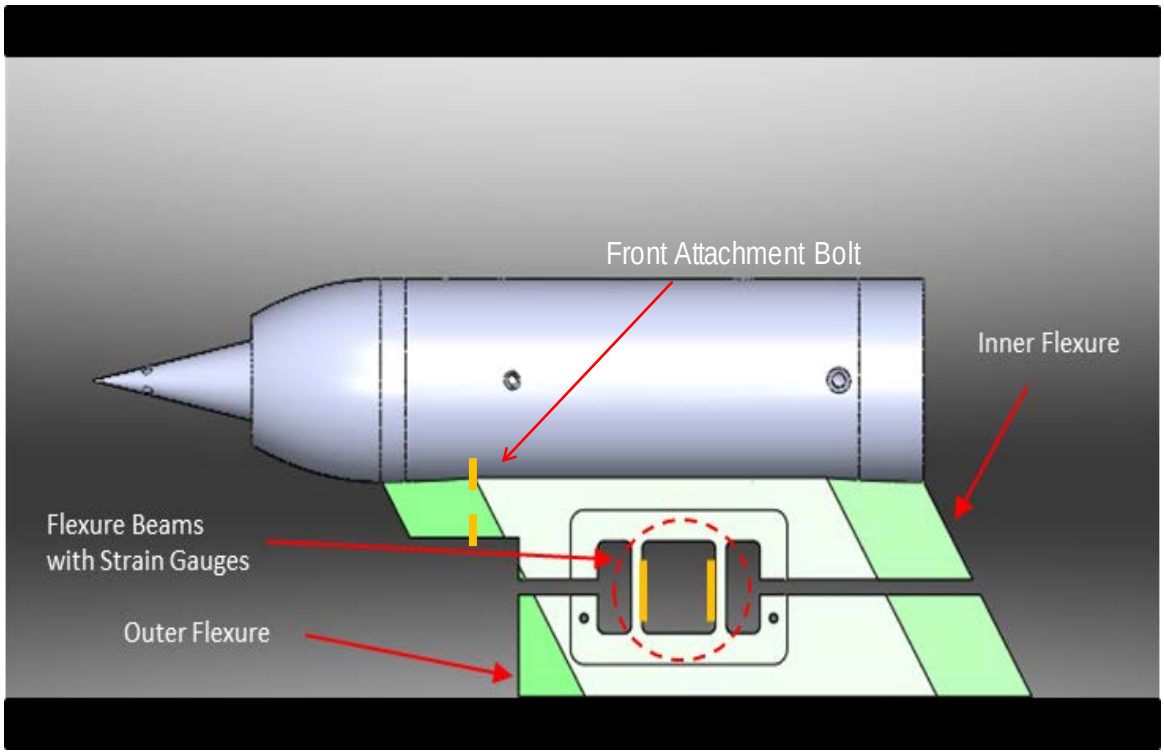

Figure 1 Model of ramjet being held in place in the SSWT by the modified flexure arm.

The assembled model with the strut is shown in Figure 2 and the model mounted in the Supersonic Wind Tunnel is shown in Figure 3 with the winglet not in view because it was mounted on the opposite side wall of the SSWT.

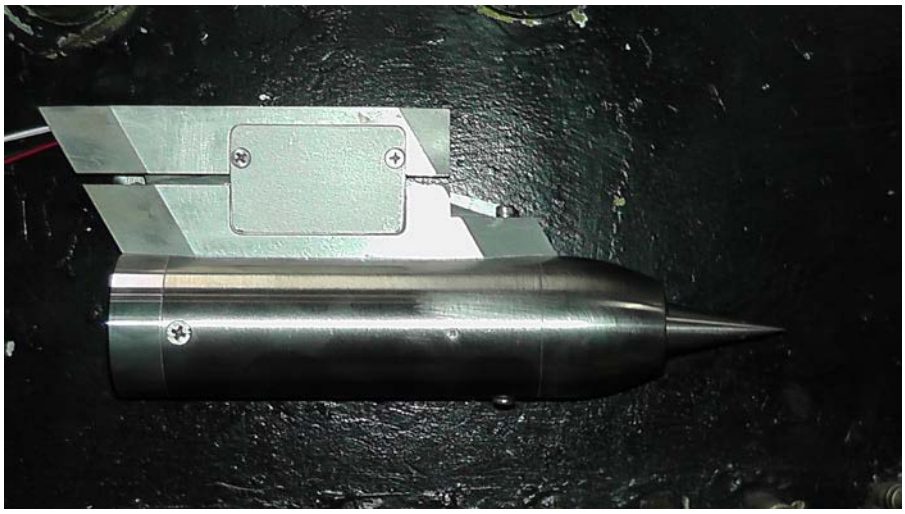

Figure 2 Ramjet connected to the winglet with strain gauges attached.

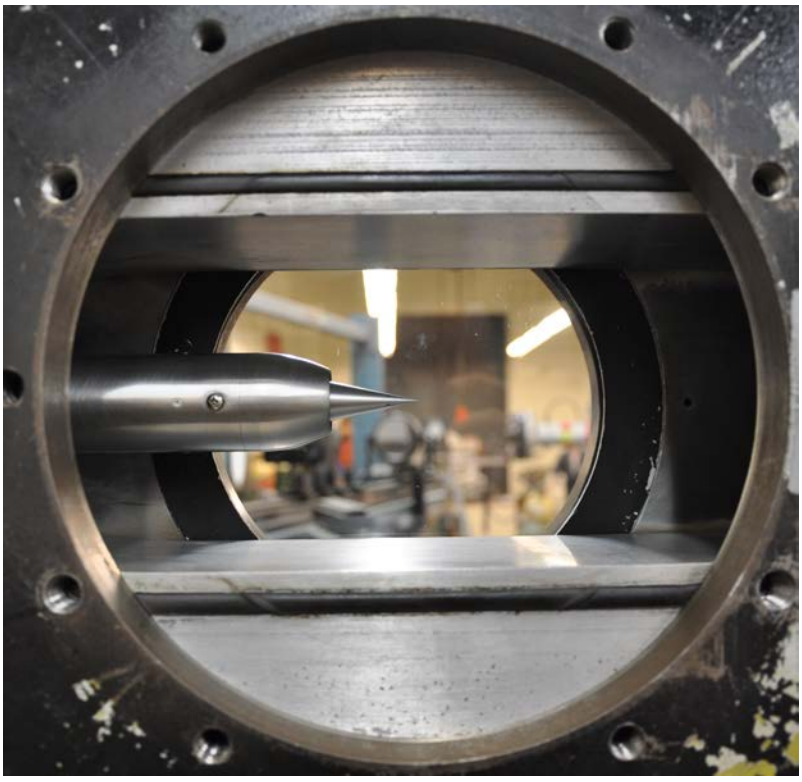

Figure 3 Ramjet mounted in the SSWT.

2. Nozzle Modifications

The same ramjet model that was used in [3] was used in these experiments. The only thing that was changed was the aft nozzle. The experiment was run with three different configurations of the nozzle which are regarded as Nozzles A, B, and C. With respect to the nozzle throat area of the nozzle used in [3], Nozzle A had the same nozzle throat area, Nozzle B had a 20 percent reduction of the nozzle throat area, and Nozzle C had a 40 percent reduction of the nozzle throat area. Engineering models for the ramjet model, including the three different nozzles, are given in Appendix A.

3. Strain Gauges Setup

The low temperatures in the operating SSWT required cryogenic strain gauges and specialized epoxy to bond the strain gauges to the flexure arms. The gauges used were Micro-Measurements WK-13062AP-350 and the epoxy used was EP29LPSP from Micro-Measurements. Whereas in [3] the strain gauges were set up in a full Wheatstone bridge configuration, which included four gauges, because of its ability to automatically compensate for large temperature fluctuations, these set of experiments could not utilize that due to only having two strain gauges in the single strut. Thus, the half-bridge configuration was used. To compensate for the temperature fluctuations, the calibration of the strain gauges was done immediately after the experiment was run so that the known forces were being applied to the ramjet while the strain gauges were at the low temperatures of the running SSWT. More details on the strain gauges can be found in Appendix H in [3]. The configuration of the strain gauges is shown in Figure 4.

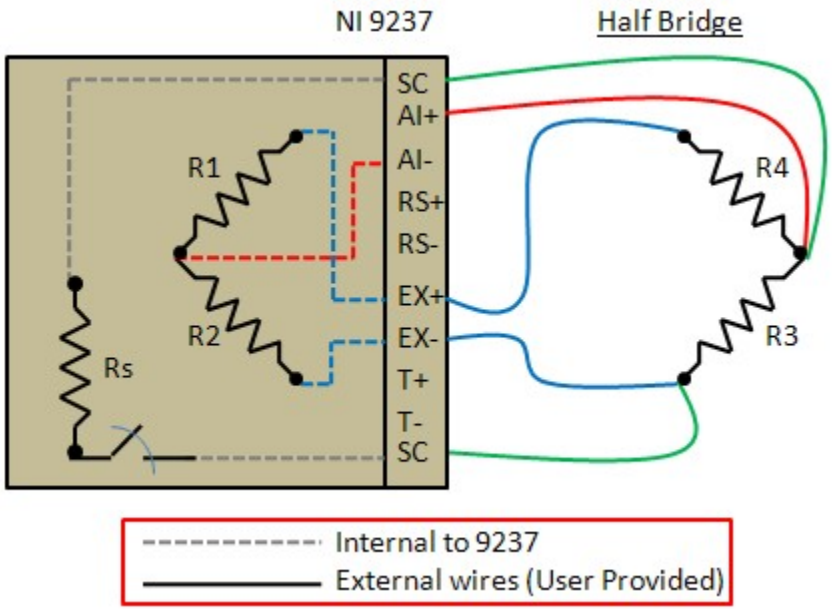

Figure 4 Connection diagram for a half bridge strain gauge configuration and NI 9237, from *NI.com*

4. Data Acquisition

National Instruments cDAQ-9181 and NI 9237 was the hardware used for measuring the outputs from the strain gauges. The wires from the strain gauge were connected to the NI 9237 through an RJ-50 wire, which transferred its measurements to the NI cDAQ-3181, which then digitized the information which was presented to and recorded by the NI MAX software. Figure 4 shows the RJ-50 wire connecting to the NI 9237, which was attached to the NI cDAQ-3181, with an Ethernet cable connecting that to a 32-bit computer with the NIMAX software running.

C. PROCEDURE

A full delineation of the details of this experimental setup is given in Appendix B. The abridged procedures given below were completed sequentially.

1. The SSWT was run at Mach 4.0 to obtain the Schlieren image and reduce the temperature of the ramjet, strut, and strain gauges close to the static temperature of the running SSWT. Hysteresis sometimes prevented the strain measurements from returning to zero after the run is complete, so the strain measurements were not always recorded for the first run.

2. After the first run and before the second run, the strain gauges were calibrated using the NIMAX software to zero the readings at the free stream velocity of zero.
3. The SSWT was run a second time to record the strain during the run, while paying particular attention to the transient between Mach 0.0 and Mach 4.0 and when the tunnel was at a steady Mach 4.0
4. Step (3) was repeated.
5. After the third run is completed, the window of the tunnel was removed so that known forces, could be applied to the nose of the ramjet so that strain could be measured and the strain-per-drag force could be calculated. The load cell used to apply these forces can be seen in Figure 5.

Figure 5 Load cell used to apply known forces to ramjet in SSWT.

D. RESULTS

Data was collected for the ramjet with all three nozzle designs. A complete listing of the drag calculations from the data collected is shown in Table 1.

	Throat Area Compared to Original Nozzle	Drag [N]		
		run 1	run 2	average
Nozzle A	100%	45.2 ± 12.1	42.9 ±	44.5
Nozzle B	80%	N/A	52.6 ± 46.9	52.6
Nozzle C	60%	46.5 ± 25.4	48.0 ± 30.0	47.3

Table 1 Tabulated results of the three different setups in the SSWT

1. Results with Nozzle A

The runs in the SSWT produced the expected Schlieren image (Figure 6) of the shock cone around the ramjet center body. The freestream velocities in the tunnel did reach the required Mach 4.0 with the static pressure and temperature in the tunnel of 8000 Pa and 68 K respectively. The strain gauges worked properly at the low temperatures in the wind tunnel and the readings returned to zero after the tunnel was shut down and the freestream velocities returned to zero. Figure 7 shows the strain during the two runs that readings were taken. The strain during the startup transient and the steady Mach 4.0 freestream velocity are shown in both runs, whereas the shutdown transient was only able to be taken during the second run. The sampling rate of the gauges and software was 5 Hz.

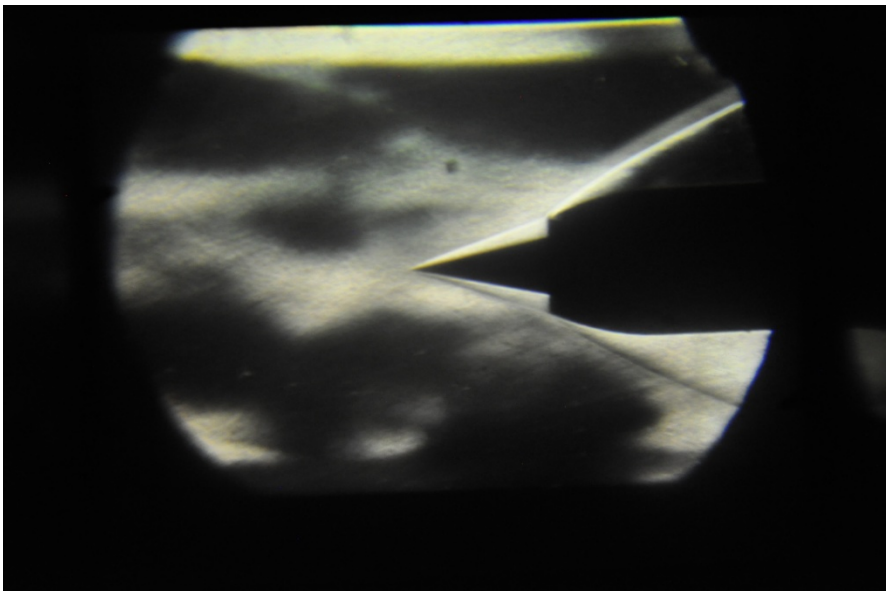

Figure 6 Schlieren image of ramjet in SSWT at Mach 4.0 with Nozzle A.

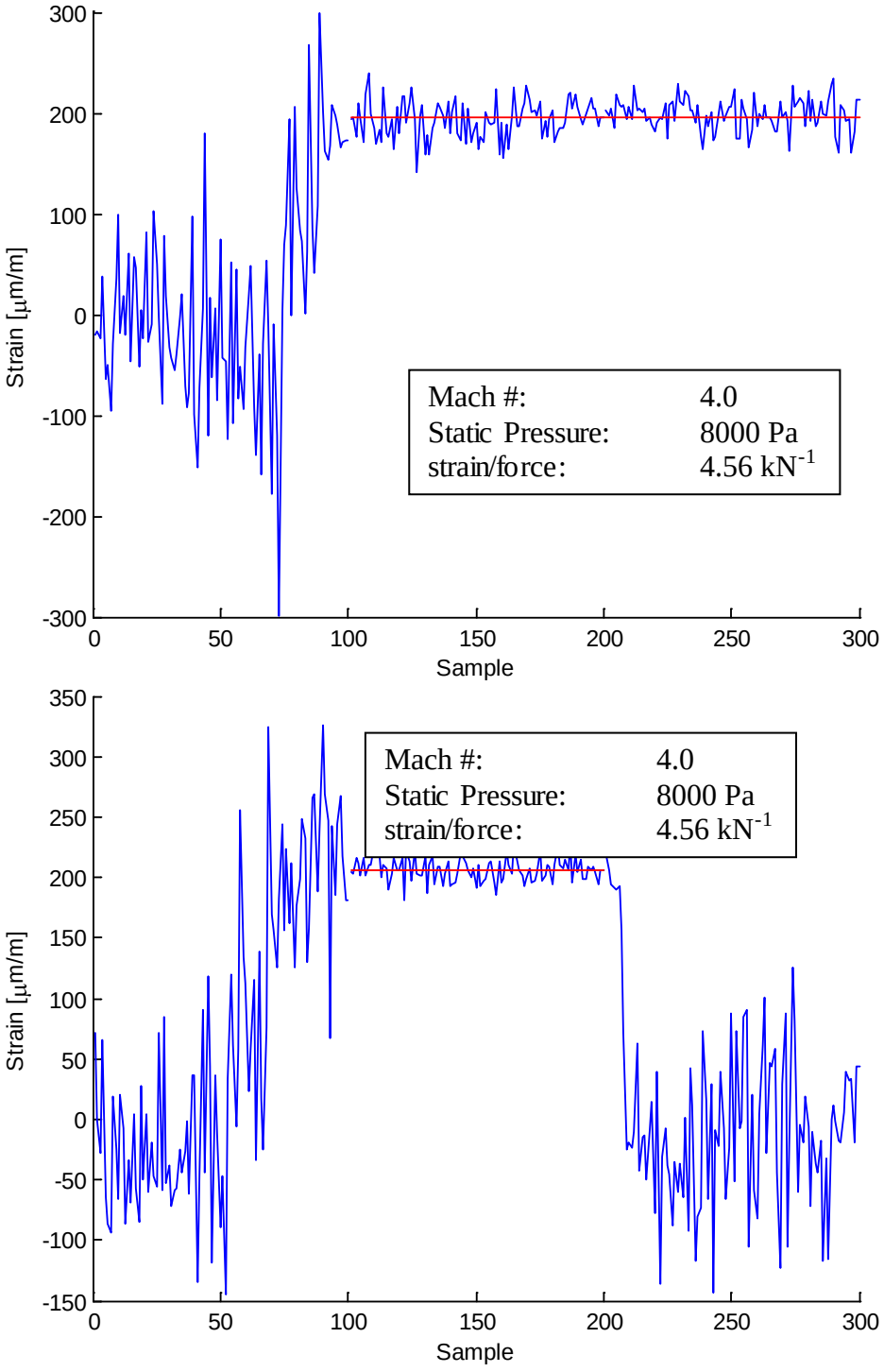

Figure 7 Steady strain readings from SSWT runs with Nozzle A.

The experiment was run on two separate days with Nozzle A with two runs completed each day. The data shown above were from the first run on the first day and the second run on the second day. The other runs that day did not produce as clear of results as those shown above. The other results are listed in Appendix C.

2. Results with Nozzle B

The SSWT functioned properly and produced the expected Schlieren image (Figure 8) of the ramjet, indicating the tunnel was working at proper conditions. Hardware malfunctions prevented the first run from being recorded, while the results of the second run are shown in Figure 9. The strain readings while the tunnel was operating at the steady Mach number of 4.0 are not as steady as those recorded with Nozzle A. This may be due to the position of the inlet shock having moved from an annular oblique shock past the inlet with Nozzle Configuration A to a normal shock at the inlet with Nozzle Configuration B. However, more testing will have to be done to confirm this.

Figure 8 Schlieren image of ramjet in SSWT at Mach 4.0 with Nozzle B.

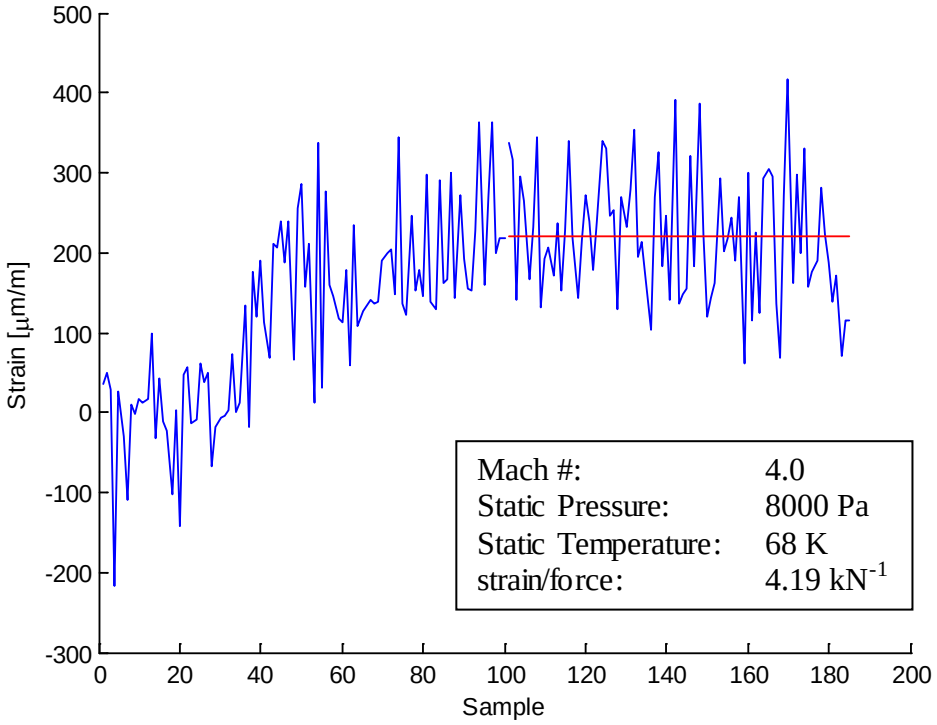

Figure 9 Strain readings from SSWT run with Nozzle B.

3. Results with Nozzle C

For the runs with the ramjet using Nozzle C, the SSWT functioned properly. A Schlieren image with a less defined oblique shock coming off the nose cone was expected due to increased back pressure from the smaller nozzle throat area causing spill out at the inlet. However this was not observed, as can be seen from comparing Figure 10 to Figure 6 and Figure 8. The observed oblique shock did indicate, however, that the SSWT did run at the required Mach 4.0. Figure 11 shows the strain results from the two runs completed using the ramjet configured with Nozzle C. Again the strain readings were not as steady as those taken when the ramjet was configured with Nozzle A. This can either be due to the inlet shock being in a different location, or can be remedied by completing more SSWT runs with this nozzle. More runs will have to be completed to determine this.

Figure 10 Schlieren image of ramjet in SSWT at Mach 4.0 with Nozzle C.

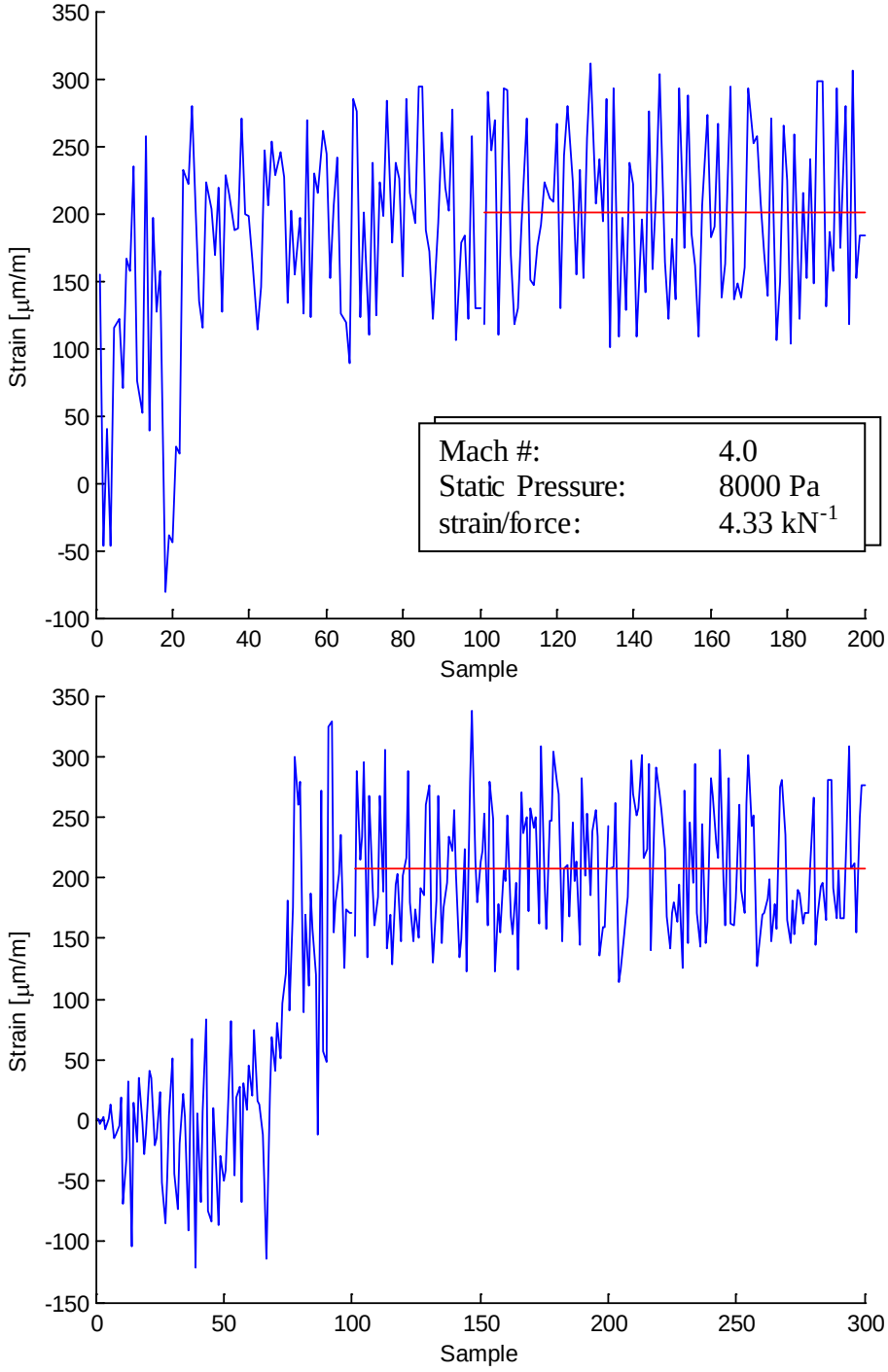

Figure 11 Strain readings from SSWT run with Nozzle C.

III. COLD-FLOW CFD ANALYSIS

A. BACKGROUND AND METHODOLOGY

In [3], a three-dimensional simulation of the ramjet in the SSWT was performed in order to predict the drag experienced. Symmetry was employed at two planes so that only one quarter of the ramjet and one of the winglets would have to be modeled, reducing computational costs. The drag calculated for the quarter ramjet and the winglet were then multiplied by 4 and 2, respectively. This introduced an inaccuracy due to the two planes of symmetry essentially accounting for four winglets in the computation, while in the experiment there were only two winglets used. In these simulations, only one plane of symmetry was employed to increase accuracy, making it necessary to only model half of the ramjet and half of the winglet.

Also in [3], analyses were done for different configurations of the nozzle. Analyses were done with a ramjet using the base nozzle design, and then with throat area reduced by 10%, 20%, 30%, and 40% from the base area. To analyze the accuracy of those computations, this thesis had two new nozzles (20% and 40% reductions in the nozzle throat area) manufactured for testing in the SSWT. Computational models of these new nozzles were also performed simulating the conditions in the SSWT.

These CFD analyses utilized SolidWorks modeling software to create the models of the ramjet with the winglet attachment as well as the SSWT section. These models were then imported into ANSYS-CFX Workbench 14.0, where a mesh was created, flow conditions were set, and the computation was run using typically 12 processors.

B. COMPUTATIONAL MODEL SETUP

1. Geometry

To exploit the axis of symmetry present on the model and winglet in the SSWT, half of the ramjet, winglet, and SSWT section were modeled utilizing the symmetry plane shown in Figure 12. The winglet was also simplified to reduce computational costs. A comparison of the physical winglet and the simplified winglet model used in the CFD analysis is shown in Figure 13.

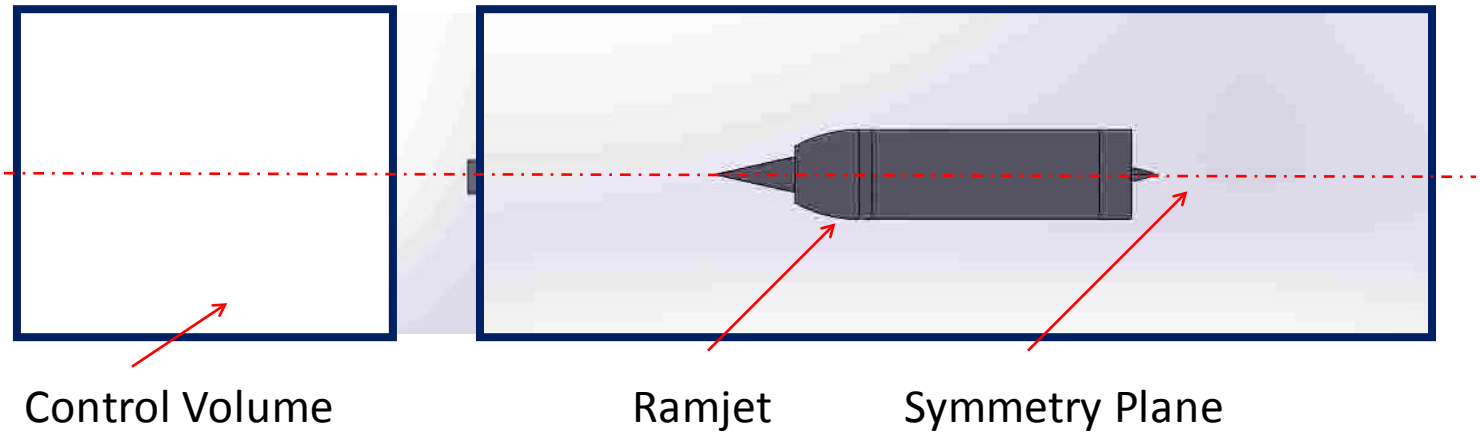

Figure 12 Ramjet model in computational domain.

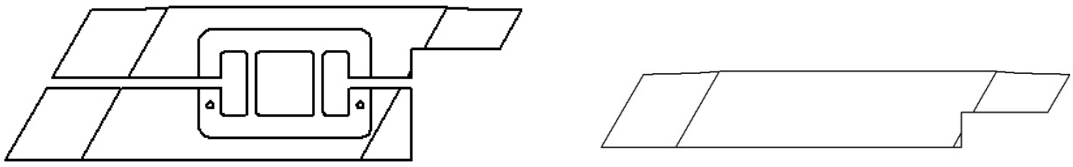

Figure 13 Comparison of physical flexure model and equivalent CFD flexure model

The ramjet, winglet, and SSWT section were modeled in SolidWorks before they were transfered into the geometry program within ANSYS. ANSYS CFX was then used to subtract the ramjet model from the SSWT test section model to create the computational domain. The computational domain is shown below in Figure 14.

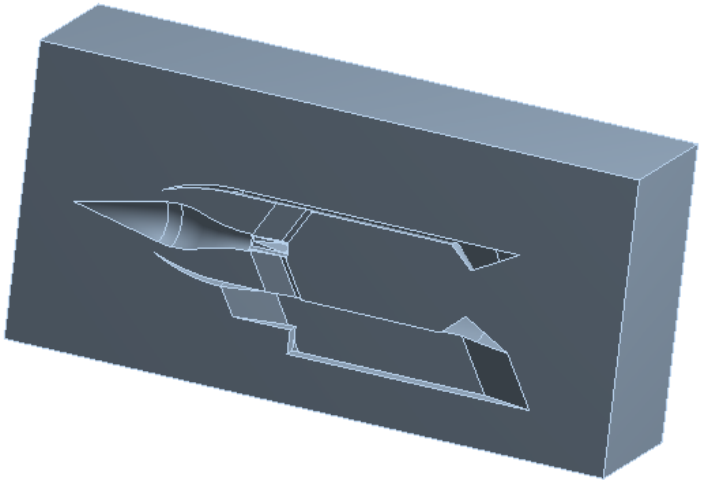

Figure 14 Computational domain of the CFD analysis.

2. Mesh

The meshing module within ANSYS was then utilized to create the computational mesh. Inflation layers were created near each wall of the ramjet and winglet. The parameters of the mesh can be found in Appendix D. For the model with the base nozzle design (nozzle A), the utility created 3.83 million nodes and 20.03 million elements. Figure 15 shows an example section of the mesh, with the smaller inflation layers visible at the nozzle/domain interface.

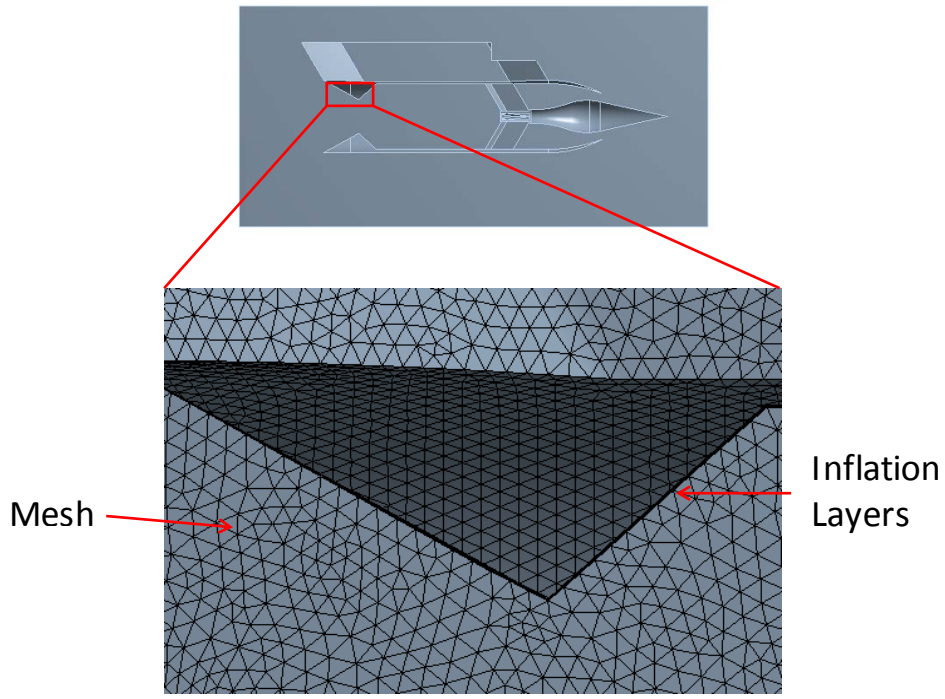

Figure 15 Close up of ANSYS generated mesh.

3. Boundary Conditions

All of the computational parameters were set up in ANSYS CFX-PRE. All of the parameters can be found in Appendix D while a snapshot can be seen in Table 2.

Boundary	Type	Boundary Condition
Inlet	Inlet	Supersonic, V = 661 m/s, P = 7378 Pa, T = 68 K
Outlet	Outlet	Supersonic
Ramjet	Wall	No-Slip Wall
Winglet	Wall	No-Slip Wall
Symmetry Planes	Symmetry	-
SSWT Sides	Wall	No-Slip Wall

Table 2 Boundary conditions of the SSWT CFD analysis.

C. RESULTS

1. Mach Profiles and Shock Locations

Figure 16 shows the Mach number profile for the whole symmetry plane and the total pressure profile at the area of the shock at the inlet cowl. This figure can be compared with Figure 5 in [3] to see the similarities between the two computational models. however, the figures in [3] do not show the winglet, as this was not included in that analysis. Figures 17 and 18 show the same Mach number profile and total pressure profile for the models with a 20% and 40% reduction in nozzle throat area respectively. They can be compared with Figures 13 and 15 in [3]. Figure 19 exhibits the shock indicators at the inlet cowl for all three setups. Comparing this with Figure 16 in [3] shows very favorable comparison between the two sets of computational simulations.

Mach Number

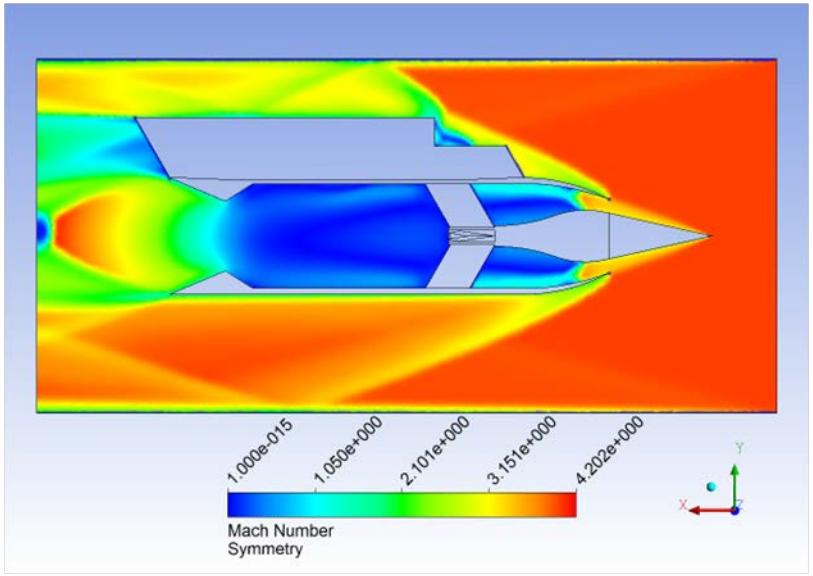

Total Pressure

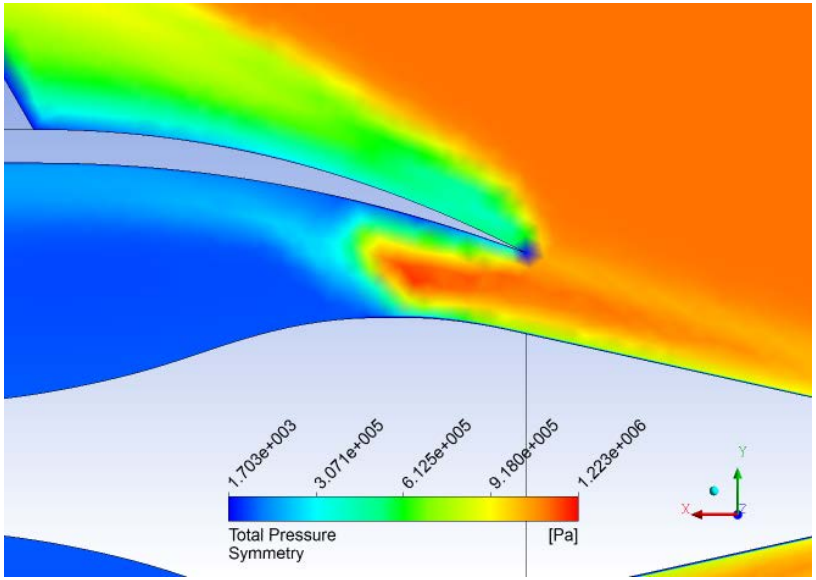

Figure 16 Mach profile and total pressure at inlet for model with 100% nozzle throat area.

Mach Number

Total Pressure

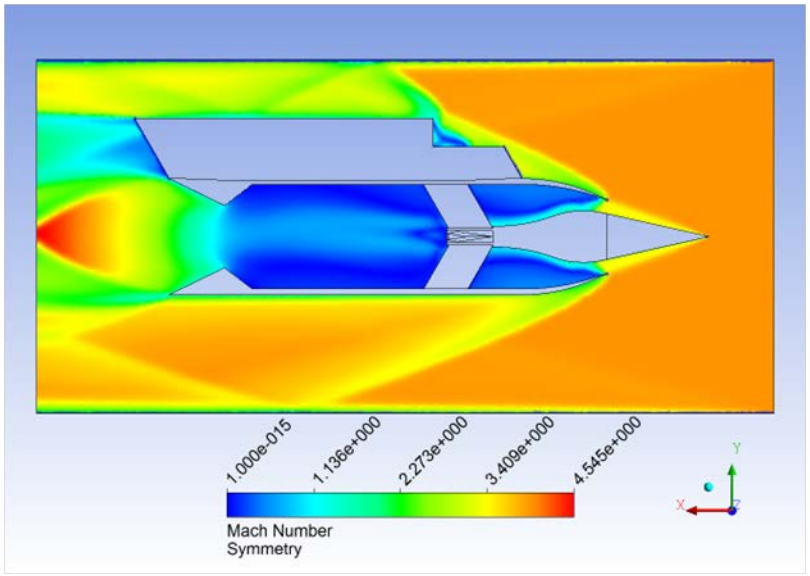

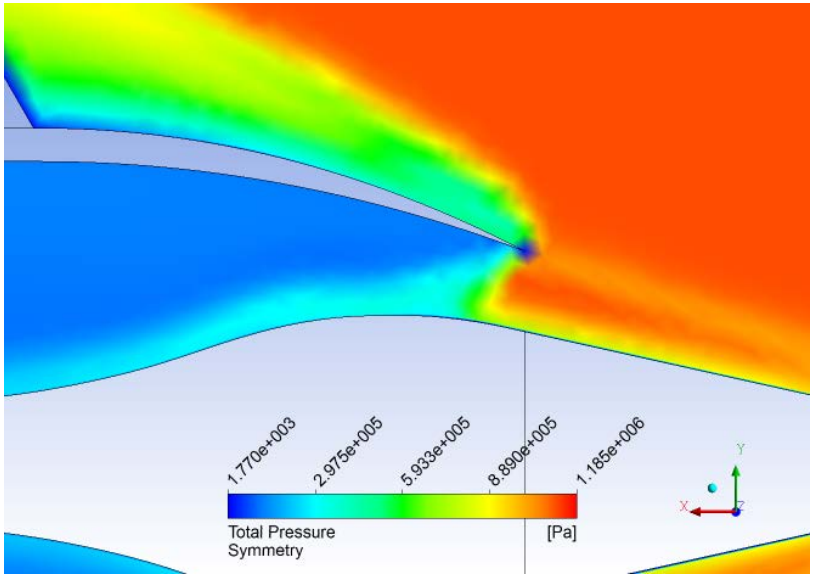

Figure 17 Mach profile and total pressure at shock for model with 80% nozzle throat area.

Mach Number

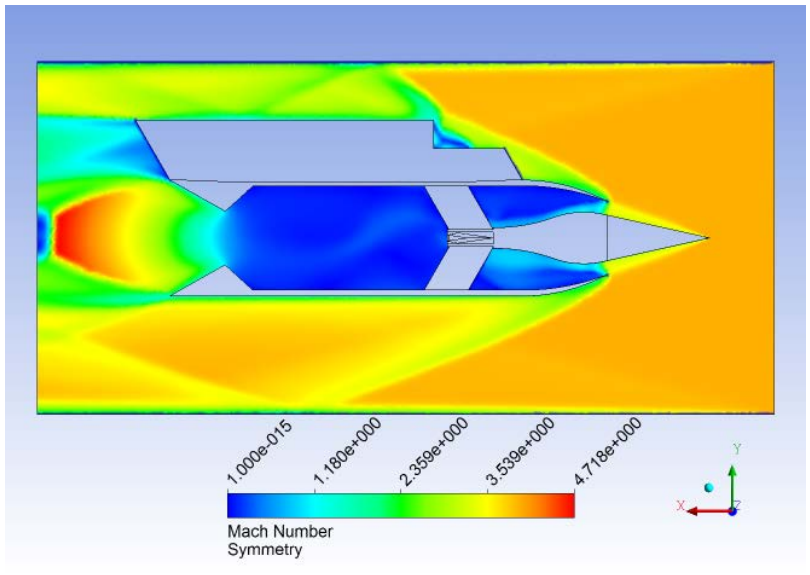

Total Pressure

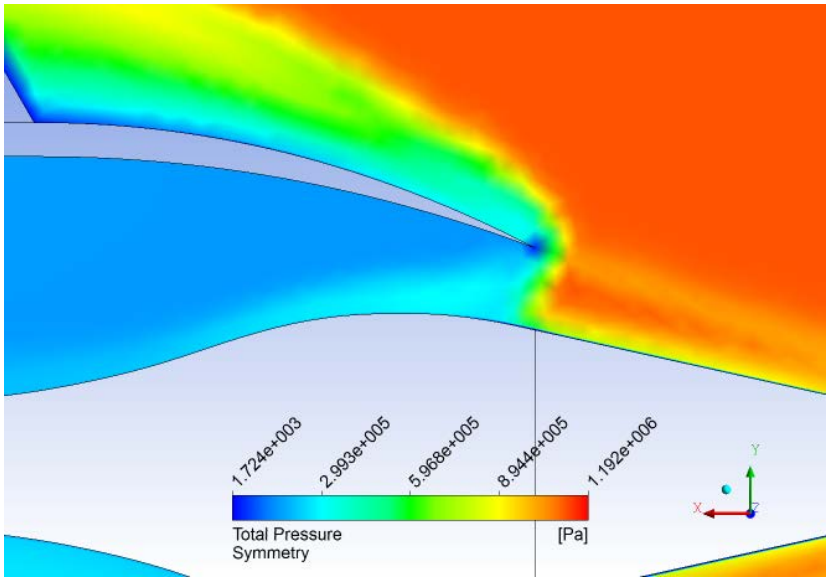

Figure 18 Mach profile and total pressure at shock for model with 60% nozzle throat area.

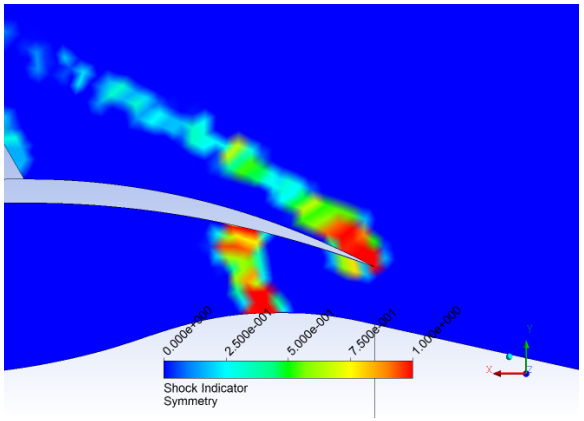

100% Nozzle Throat Area

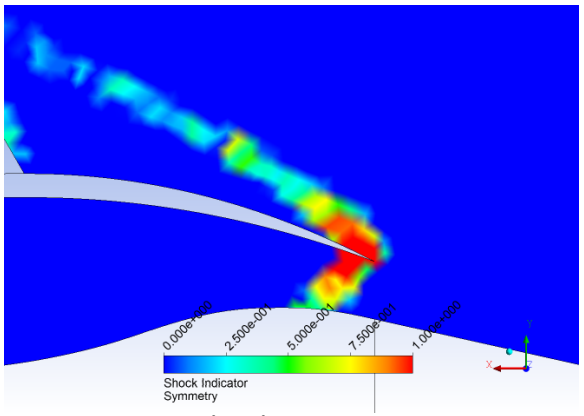

80% Nozzle Throat Area

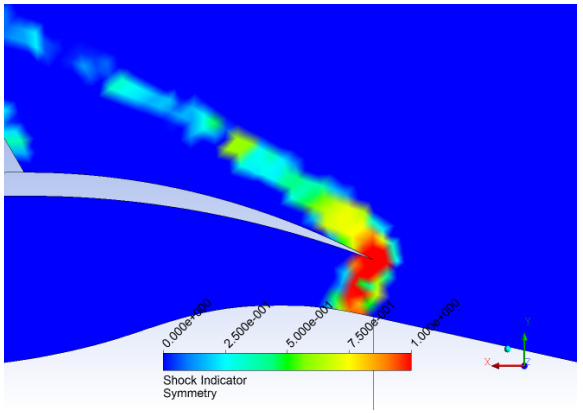

60% Nozzle Throat Area

Figure 19 Shock indicator profiles at inlet cowling.

2. Drag Predictions

Drag calculations of each model were able to be completed using the ANSYS CFX-Post function calculator. The drags on each of the configurations are listed in Table 3. A property of interest when predicting drag on a surface is the dimensionless wall distance, or y^+, defined as $y^+ = \left(\sqrt{\frac{\tau_w}{\rho}}\right)\frac{y}{\nu}$, where τ_w is the wall shear stress, ρ is the fluid density, y is the distance from the wall, and ν is the kinematic viscosity. A y^+ value between 1.0 and 3.0 indicates that the calculated values close to the walls are accurate. The y^+ values for these computational models, shown in Table 4, are small enough to assume accurate computational measurements at the walls.

Model	Nozzle Throat Area Compared to Base Design	Drag on Half Ramjet	Drag on Half Winglet	Total Drag
A	100%	13.36 N	5.33 N	37.38 N
B	80%	12.63 N	5.42 N	36.10 N
C	60%	14.73 N	5.31 N	40.08 N

Table 3 Computational drag measurements.

Model	Nozzle Throat Area Compared to Base Design	y^+ Ramjet	y^+ Winglet
A	100%	1.63	1.198
B	80%	1.869	1.31
C	60%	1.965	1.316

Table 4 Average y^+ values for surfaces in computational models.

D. COMPARISON OF EXPERIMENTAL MEASUREMENTS AND COMPUTATIONAL PREDICTIONS

The results of the drag measurements for both the SSWT experiments and the ANSYS CFX simulations are tabulated in Table 5. These results show that the drag on the model with nozzles A and C were consistently under predicted by the computational models by around 14 percent. The one run that was able to be completed on the ramjet with nozzle B showed significantly more drag than the others. The comparison of the experimental drag measurements on the ramjet with Nozzle B with the drags experimentally measured on the other ramjet configurations as well as the computational models led to the conclusion that the drag measured on the ramjet with nozzle B included some source of error that led to such high drag on the ramjet. The disparity between the experimental and the computational should be more consistent between nozzle configurations.

Model	Nozzle Throat Area Compared to Base Design	Experimental Drag Measurement	Computational Drag Measurement	% Error
A	100%	42.9 - 45.2	37.38	13.0 - 17.4
B	80%	52.6	36.10	31.4
C	60%	46.5 - 47.3	40.08	13.8 - 15.2

Table 5 Comparison of experimental measurements and computational drag predictions.

THIS PAGE INTENTIONALLY LEFT BLANK

IV. COMBUSTION CFD ANALYSIS

A. BACKGROUND AND METHODOLOGY

In [2], a simplified attempt to model combustion in the ramjet using propane and oxygen at low speeds was conducted. Limitations in this approach led [3] to attempt a three dimensional CFD analysis of hydrogen fuel/air combustion in a 45 degree wedge of the ramjet utilizing symmetry planes and injection velocities of 400 m/s. That attempt failed to converge to a solution.

The results of these past attempts have pushed for the need of a better understanding of the processes and accuracy of combustion modeling on CFD software. M. J. Foust et al. of Pennsylvania State University, Reference [4], conducted physical and computational experiments on hydrogen and oxygen combustion in a rocket combustor tube. The model was very simple to allow for CFD validation, thus it was repeated in an attempt to validate the accuracy of the CFD models used in this thesis.

Using simplified geometry files derived from the SolidWorks models used to create the drawings for machining, a domain and mesh were generated using ANSYS 14.0 software. Parameters were then set, the solution was run using the processor cluster Hamming on the Naval Postgraduate School campus, and the solution was analyzed.

Once the computational model used to simulate combustion was analyzed and its utility validated, the lessons learned were incorporated into an attempt to model combustion in the combustion chamber of the ramjet. Where previous attempts were to only analyze flow in the ramjet and neglect the flow outside the ramjet, these simulations included the domain outside the ramjet in order to both try to achieve convergence in the calculations and to be able to measure drag and thrust on the ramjet body. Preliminary results were thus formed and analyzed.

B. COMPUTATIONAL MODEL VALIDATION

1. Objective

The purpose of this computational simulation was to generate results for hydrogen/oxygen combustion in a rocket engine that sufficiently match the results of computational and physical models run in 1996 [4]. This was to determine its validation of ANSYS CFX computational software effective computing the flowfield characterization of combusting hydrogen at high velocities. This would allow ANSYS CFX to be reliably used to compute the characterization of flowfields of other contexts, specifically, the miniature ramjet engine.

2. Experimental Setup

Simulating flow in the rocket engine first required a geometric model of the combustor. This was done in SolidWorks and with relative ease due to the simple geometry of the combustor. The geometric model was then uploaded into ANSYS CFX. A computational mesh was created paying close attention to both the inlets and the locations where combustion should first take place in the flow. CFX Pre was opened and the hydrogen/oxygen combustion model was then uploaded into the system setting the oxygen mass flow rate to 0.042 kg/s, and the hydrogen mass flow rate to 0.0103 kg/s [4]. The parameters for the computational setup, delineated in Appendix E, were then set to ensure the best chance for combustion to occur. When all the parameters were configured, the simulation was run, using Platform MPI Local Parallel with 6 partitions. When the computation was done running, the results were analyzed paying particular attention to the temperature and flamelet profiles and the molar fractions at locations 25.4 mm and 127 mm from the inlets, which were the initial and final measurement locations reported by Foust et al. [4].

The simple, three-species combustion, eddy-diffusivity model was used. This consisted of the following chemical equation:

$$H_2 + \frac{1}{2} O_2 \rightarrow H_2O$$

This model used transport equations for H_2, O_2, and H_2O. To initiate combustion a small amount of H_2O (0.5%) had to be injected into the O_2 stream. The complete list of boundary conditions, meshing parameters, and fluid flow setup can be found in Appendix F.

3. Results

As the results below show, the ANSYS simulations showed remarkably close resemblance to the physical experimentation done by Foust et al. [4]. One thing that was more difficult to match was their flamelet profile. The one shown below in Figure 20 is the closest to flamelet closure that could be reproduced. In earlier simulations, the flamelet would expand radially outwards from the injector ports and would not come to closure into the center of the combustor tube. However, it is likely that the present simulation was more accurate than the simulation done by Foust et al. [4]. The simulation run by them was a two dimensional representation that reported zero percent molar fraction for H_2O and H_2 at the point that they were reporting flame closure. Figure 21 and Figure 22 below shows that this simulation and Foust's et al. simulation show marked similarity in the molecular molar fractions 25.4 mm from the injector ports. However, the below simulation exhibits noticeably reduced oxygen molar fractions at the center of the tube 127 mm from the injector ports, shown in Figure 22. This should be expected if there was in fact flame present at that location. Thus, this three dimensional representation of the rocket combustor tube should bear a closer resemblance to the actual, physical model. However, the levels of inlet turbulence and length scales needed to be set to the following values: fractional intensity of 0.2 and eddy length scale of 0.02 [m] for both the O_2 and H_2 inlets. Sampling different turbulence length scales proved that the inlet conditions have to be tailored to fit the desired flamelet profile, sometimes resulting in length scales that are larger than the inlet diameter. The results of this simulation show that if the inlet turbulence and length scales are set to achieve the desired flamelet profile, the output of the simulation will adequately represent actual combustion. This observation validated the three species combustion, eddy-diffusivity model and allowed it to be further used to predict the combustion profile in the miniature ramjet.

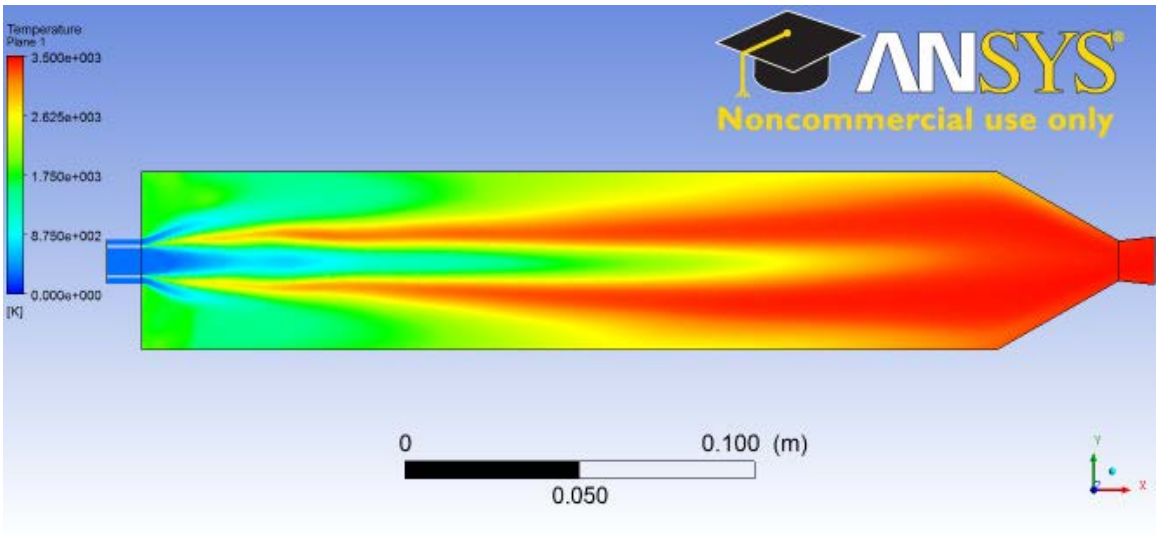

Figure 20 Predicted temperature profile.

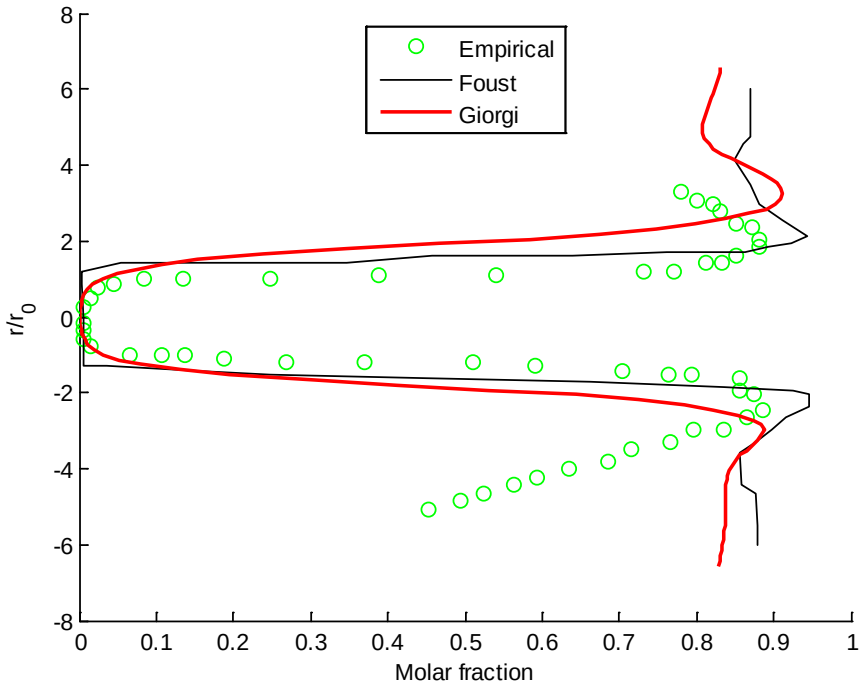

(a)

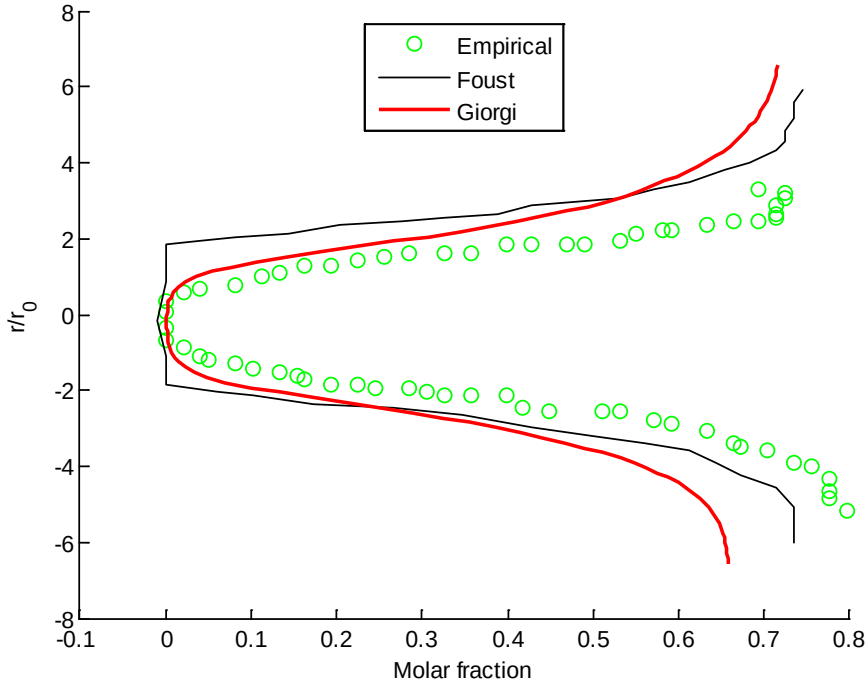

(b)

Figure 21 Molecular hydrogen mole fraction profiles at (a) 25.4 mm and (b) 124 mm from the inlets. After [4].

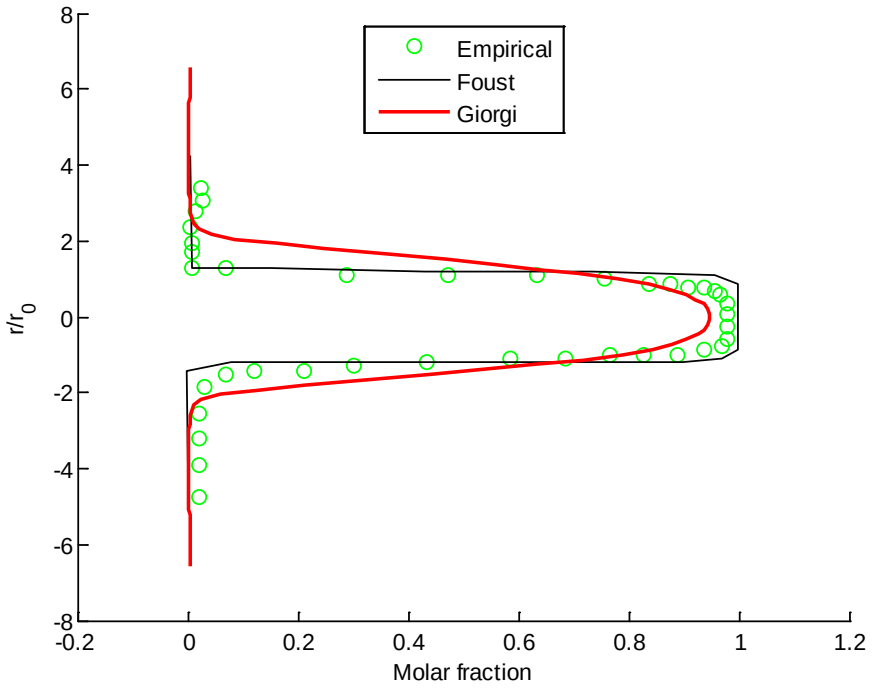

(a)

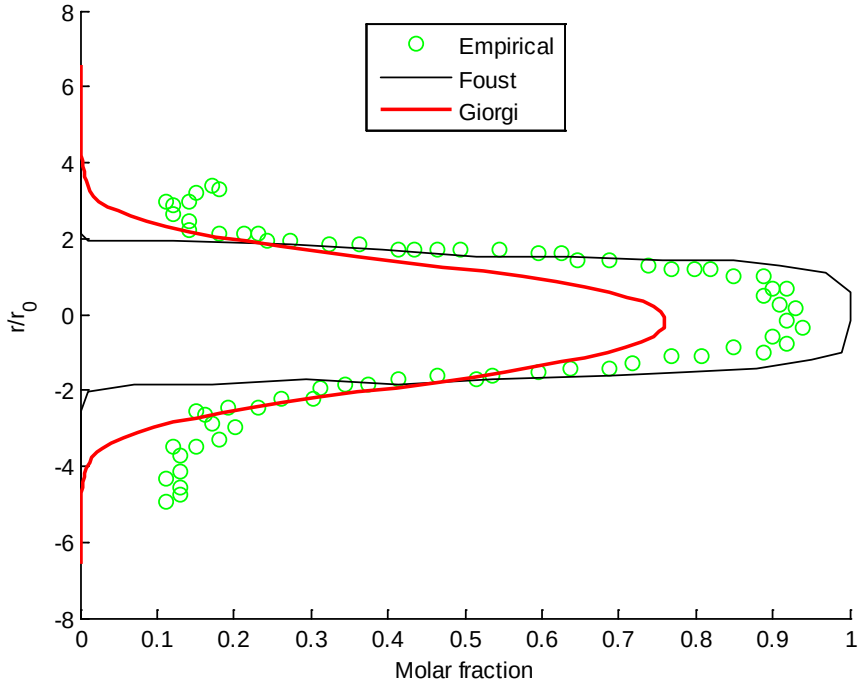

(b)

Figure 22 Molecular Oxygen mole fraction profiles at (a) 25.4 mm and (b) 124 mm from the inlets. After [4].

C. RAMJET COMBUSTION

1. Three Dimensional Setup

The symmetry planes of the ramjet were utilized to create a smaller computational domain. While only one eighth of the ramjet could have been modeled using symmetry planes, in order to fully observe the flow around the injection struts, a quarter model of the ramjet was used. Figure 23 shows the computational domain as well as the symmetry planes that were used to render it. In [3], the external flow past the inlet were excluded from the computational analysis. This simulation included them with the rationale that it would indeed help the solution to converge and allow drag to be recorded using the function calculator.

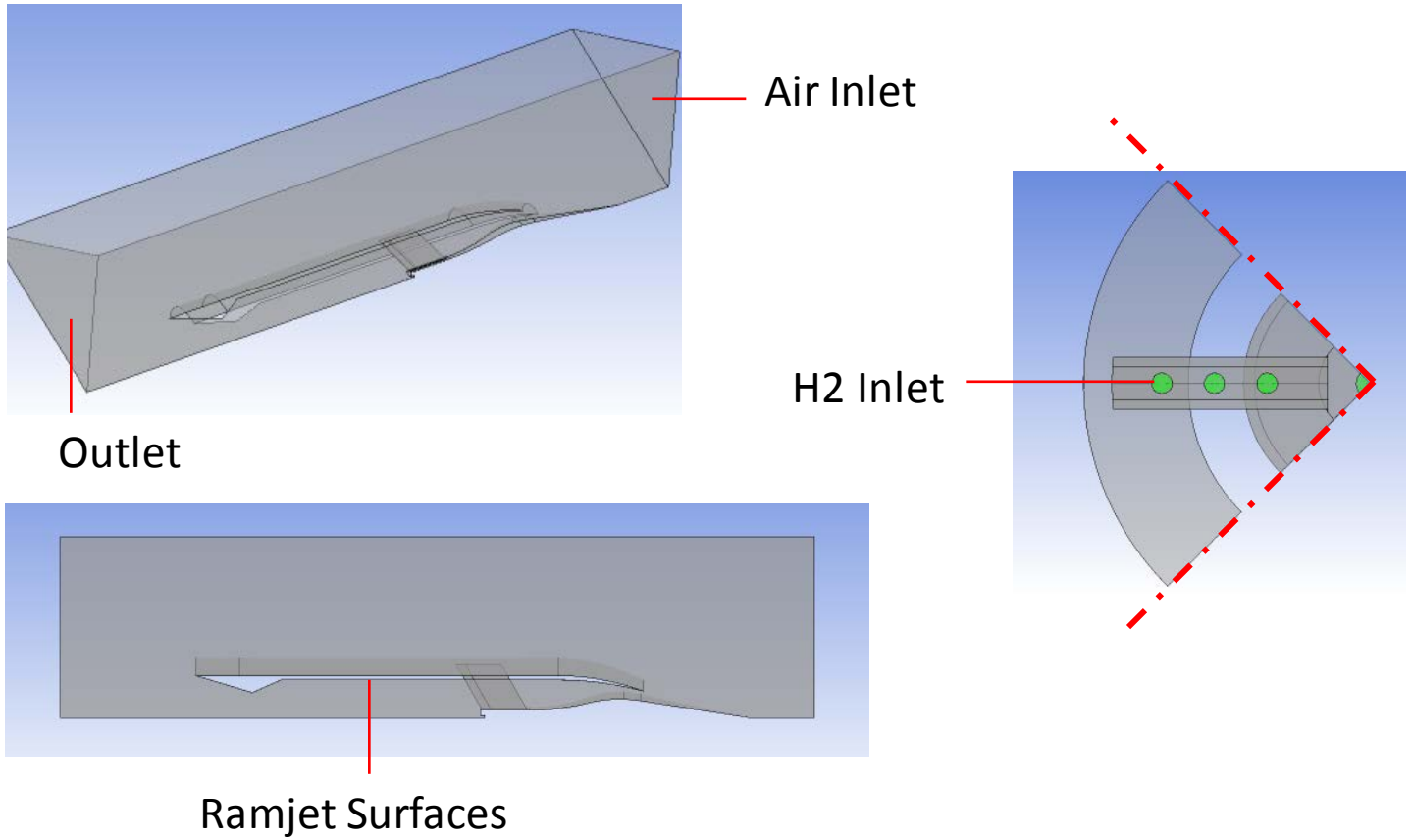

Figure 23 Computational domain of the ramjet combustion model.

The domain was meshed using inflation layers at the ramjet surfaces. The meshing parameters can be found in Appendix E. When meshing was completed, the domain contained 2.02 million nodes and 10.35 million elements.

2. Computational Domain Setup

The setup in CFX-Pre utilized the Eddy Diffusivity Model for combustion that was tested in the Computational Model Validation section. Before combustion was turned on in the computational model, a cold-flow solution was first obtained by leaving the Eddy Diffusivity Model off and setting the hydrogen flow rate to 0 meters per second. Once a cold flow solution was obtained that presented a reasonable shock structure located near the inlet cowl, then the hydrogen flow rate was set to 50 meters per second and the combustion option was set to Eddy Diffusivity Model. A complete report on the initial conditions and setup parameters can be found in Appendix F.

3. Results

The solution converged in the manner shown in Figure 24. The cold flow solution was achieved during loop iterations 1-821. Combustion was turned on at loop iteration 822 with a hydrogen flow rate at the injection ports of 50 m/s. At loop iteration 1,128, the hydrogen flow rate was increased to 75 m/s.

The results of the computational model showed that combustion did take place with a maximum temperature in the ramjet of 1,717 K as shown in Figure 25, indicating that the flame temperature did not reach the adiabatic flame temperature of 2,430 K for hydrogen/air combustion at the stoichiometric mixture ratio. This may be due to a lack of sufficient amount of hydrogen coming into the domain at the injection ports. At loop iteration 1,127, the last before the hydrogen flow rate was increased to 75 m/s, the maximum temperature was 1,436 K. This indicates that increasing the hydrogen flow rate can potentially raise the maximum temperature in the ramjet, with the potential to reach the expected adiabatic flame temperature of hydrogen/air combustion.

As can be seen in Figure 26, the flame holder appears to be at the location between the center injection port located on the center body and the centermost injection port located on the injector strut.

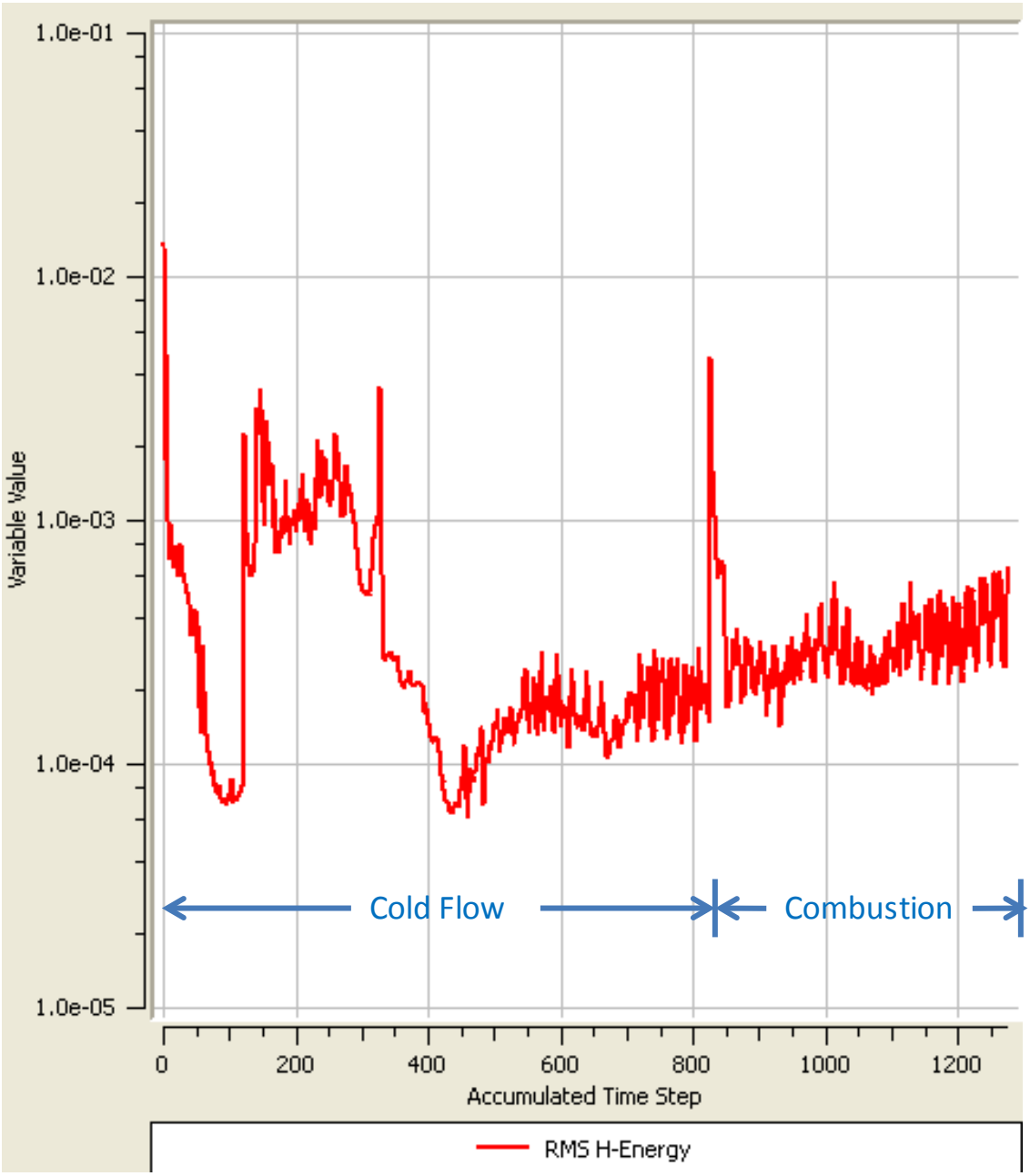

Figure 24 Heat transfer convergence history for CFX ramjet combustion model.

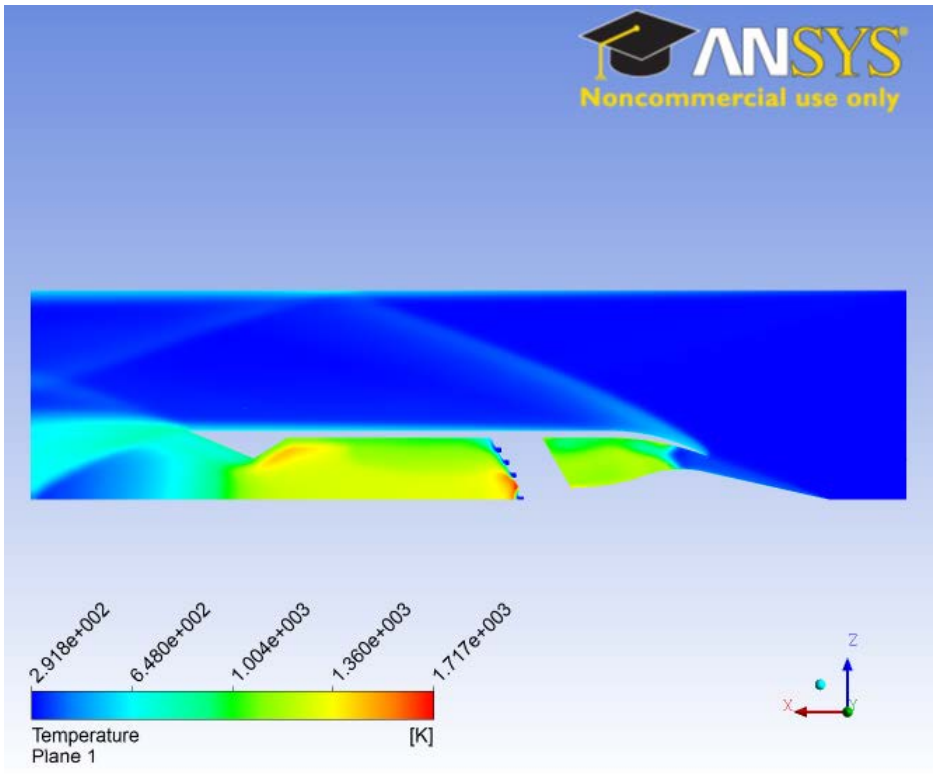

Figure 25 Temperature profile for the entire ramjet modeling combustion.

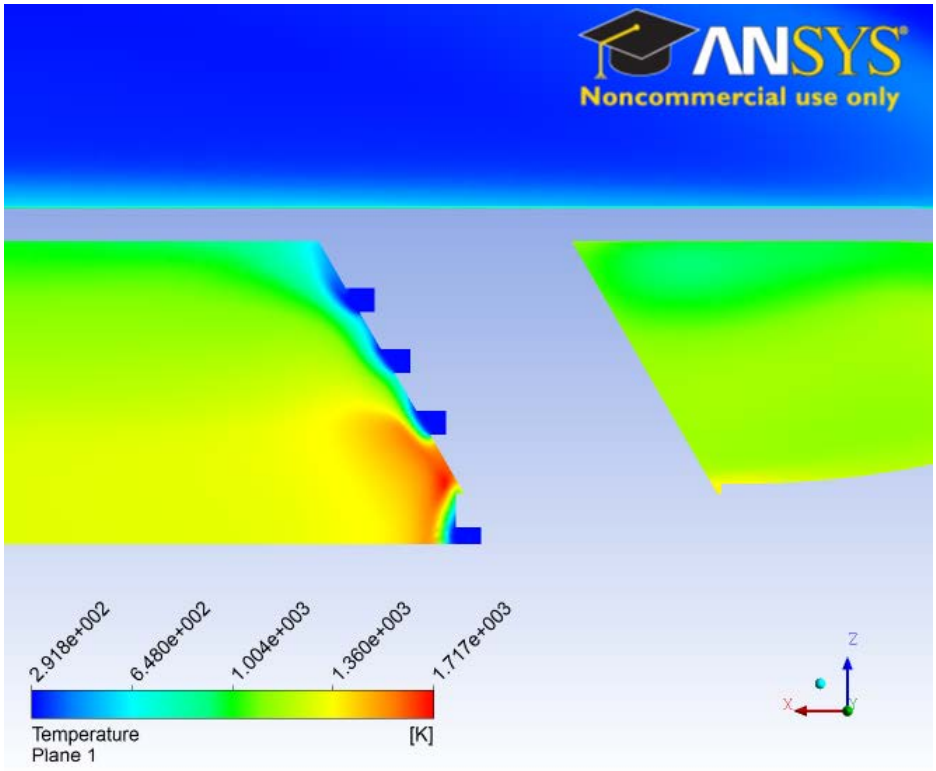

Figure 26 Temperature profile focused in on the injection ports.

V. CONCLUSIONS AND RECOMMENDATIONS

A. SUPERSONIC WING TUNNEL EXPERIMENT

The problems that were faced in [2] and [3] were not experienced in this past round of experiments. The strain gauges used worked sufficiently to produce reliable readings. Also, the use of only one winglet to mount the ramjet in the SSWT combined with the more user-friendly National Instruments Data Acquisition System proved successful in eradicating the hysteresis problem, enabling the strain reading to return to zero after the flow velocity in the SSWT returned to zero. The success of overcoming these problems having been solved as well as the strain data being as consistent as it was at the test Mach numbers has led to the conclusion that the data collected for the drag on the baseline ramjet (Nozzle A) was accurate.

As was already discussed, the strain readings taken for the ramjet configured with Nozzles B and C did not produce as neat and steady results as those readings taken on the ramjet when it was configured with Nozzle A. More tests should be run in the SSWT with Nozzles B and C to refine the data for these nozzles.

B. COLD FLOW CFD ANALYSIS

The simulations completed ran smoothly and produced more precise results. It has already been recommended that the ramjet configured with Nozzle B should be tested in the SSWT to refine the data and determine if the 52.61 N drag measured is in fact in error and should be closer to the 42.0 N expected as the computational model consistently under predicted the drag by about 14 percent. If further tests on Nozzle B do produce the expected results, then the computational model is precise enough to use it to predict drag at atmospheric conditions. Inlet and ambient conditions should be altered to model atmospheric conditions at sea level.

C. COMBUSTION CFD ANALYSIS

The results collected are only preliminary. What has been shown is that the solution is capable of converging to a solution. Thus, further work should be done to computationally model combustion in the ramjet. Currently the injection ports are only

located in the injector struts and the center body. The data collected shows that these locations appear to be sufficient for both holding the flame in place and thoroughly combusting the fuel before it exits the nozzle, however, this cannot be said with certainty because the simulations run have not been at the designed hydrogen inlet velocities.

APPENDIX A: ENGINEERING DRAWINGS FOR RAMJET MODEL

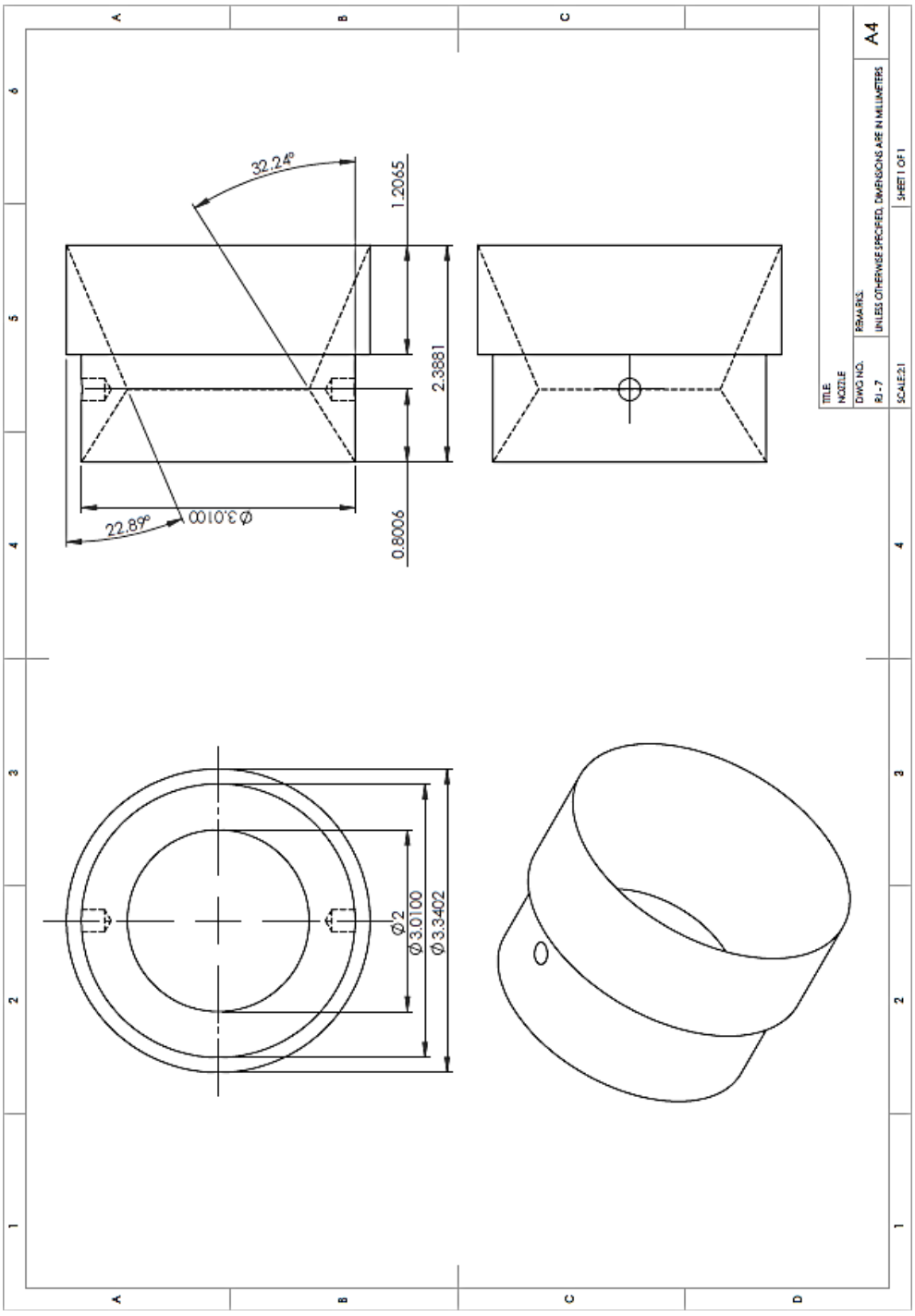

Figure 27 Part drawing: original ramjet nozzle (RJ – 7a). From [3].

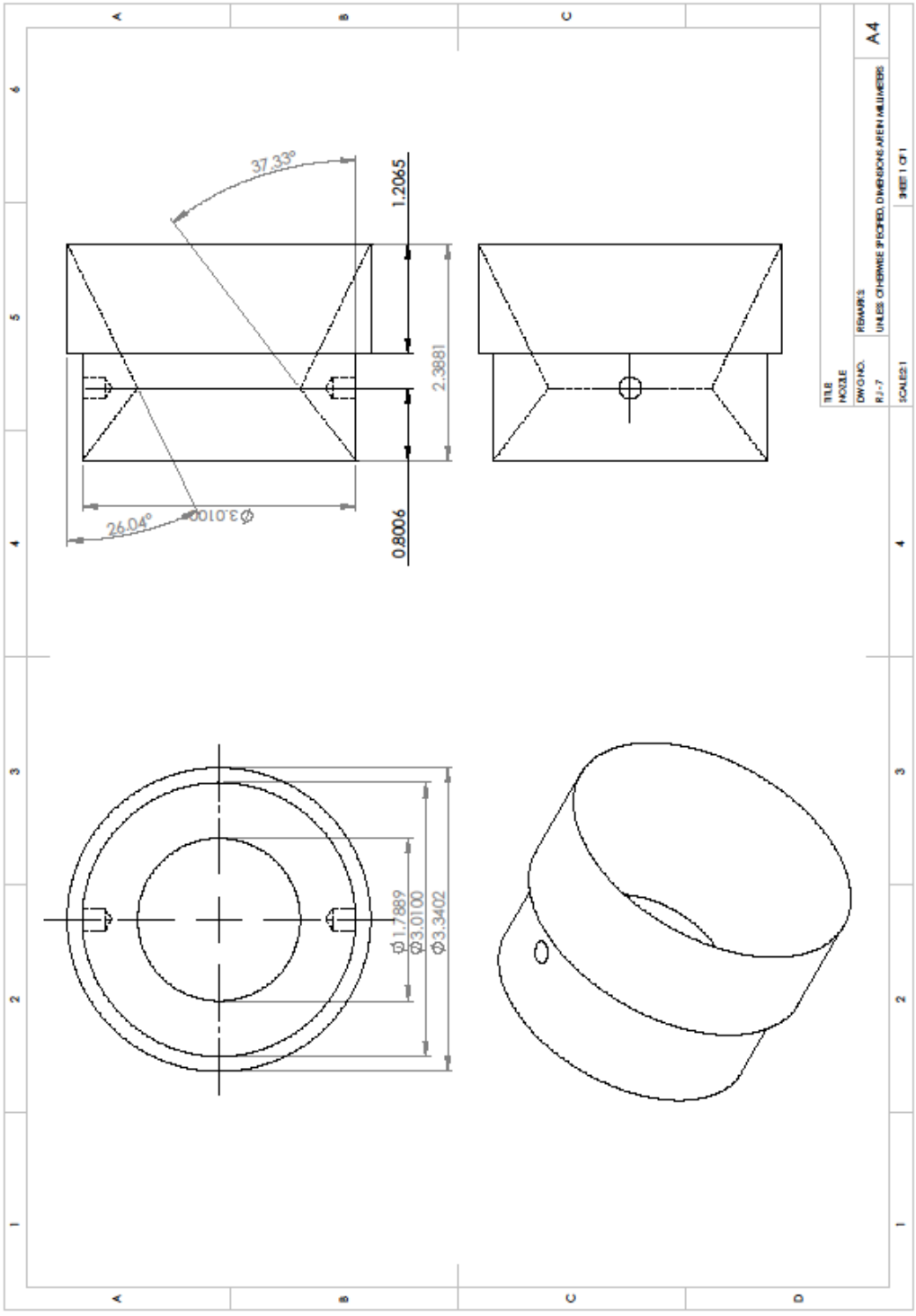

Figure 28 Part drawing: Ramjet Nozzle with 20% reduced throat area (RJ – 7b). After [3].

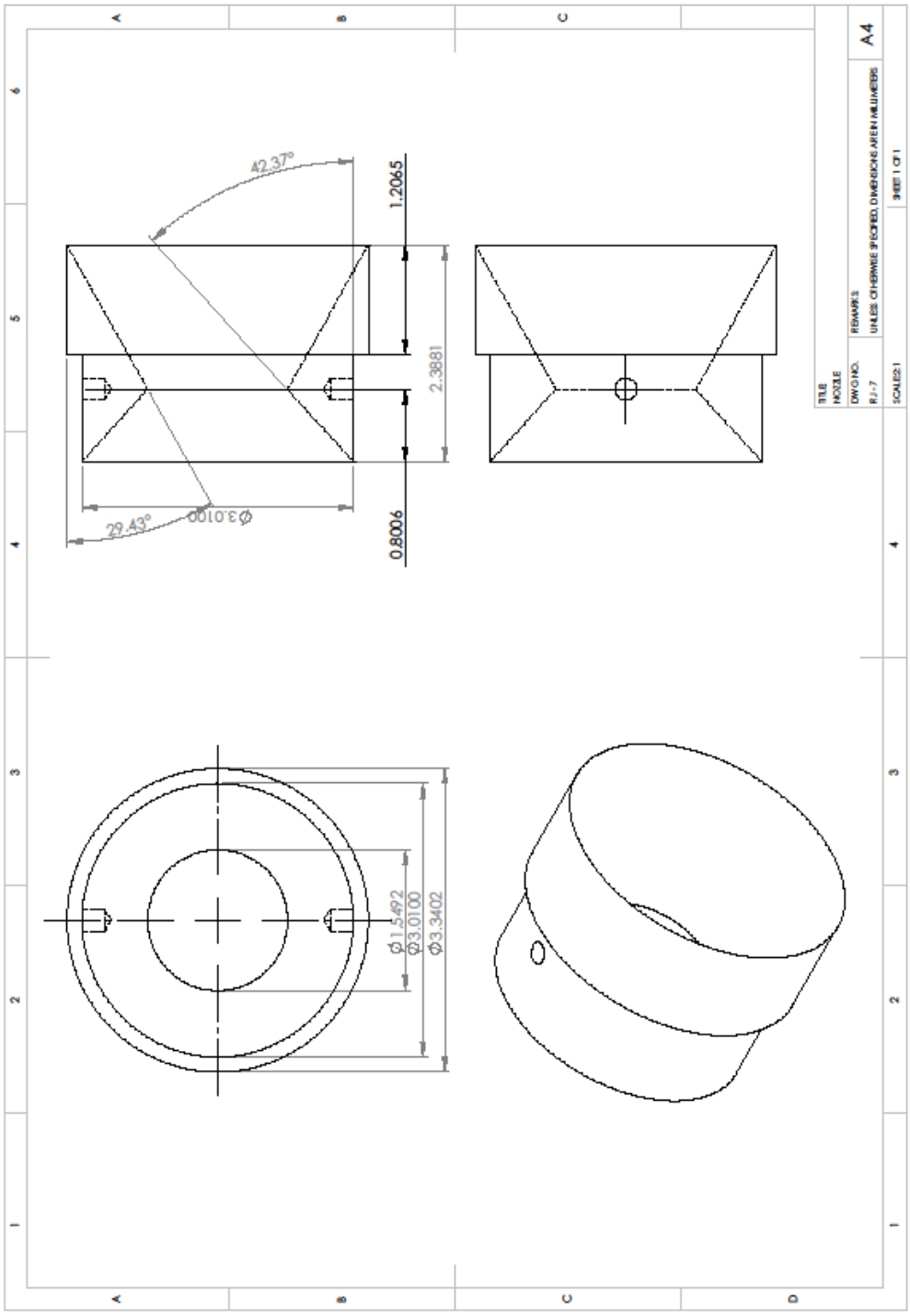

Figure 29 Part drawing: ramjet nozzle with 40% reduced throat area (RJ – 7c). After [3].

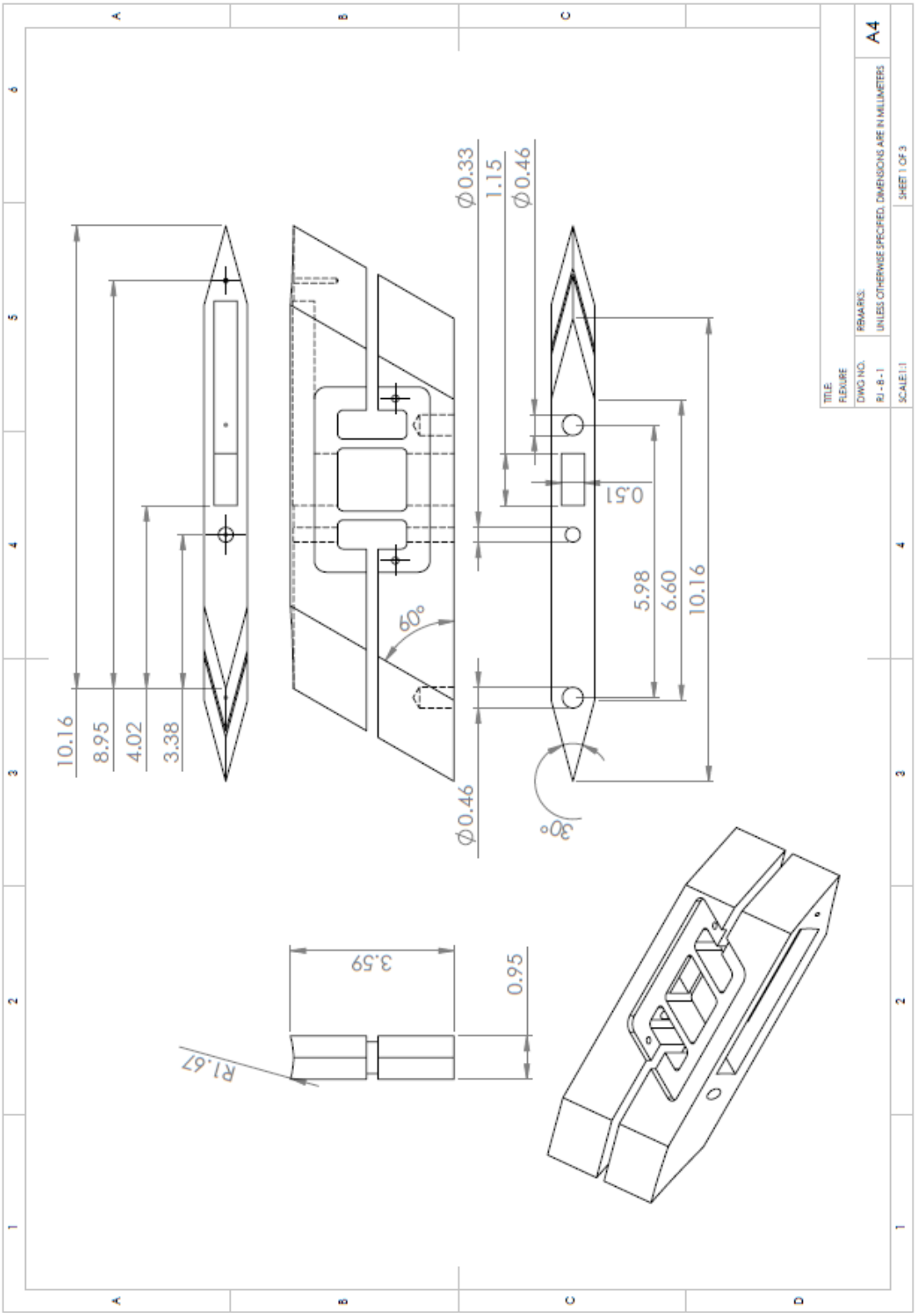

Figure 30 Part drawing: original flexure (RJ – 8 – 1). From [3].

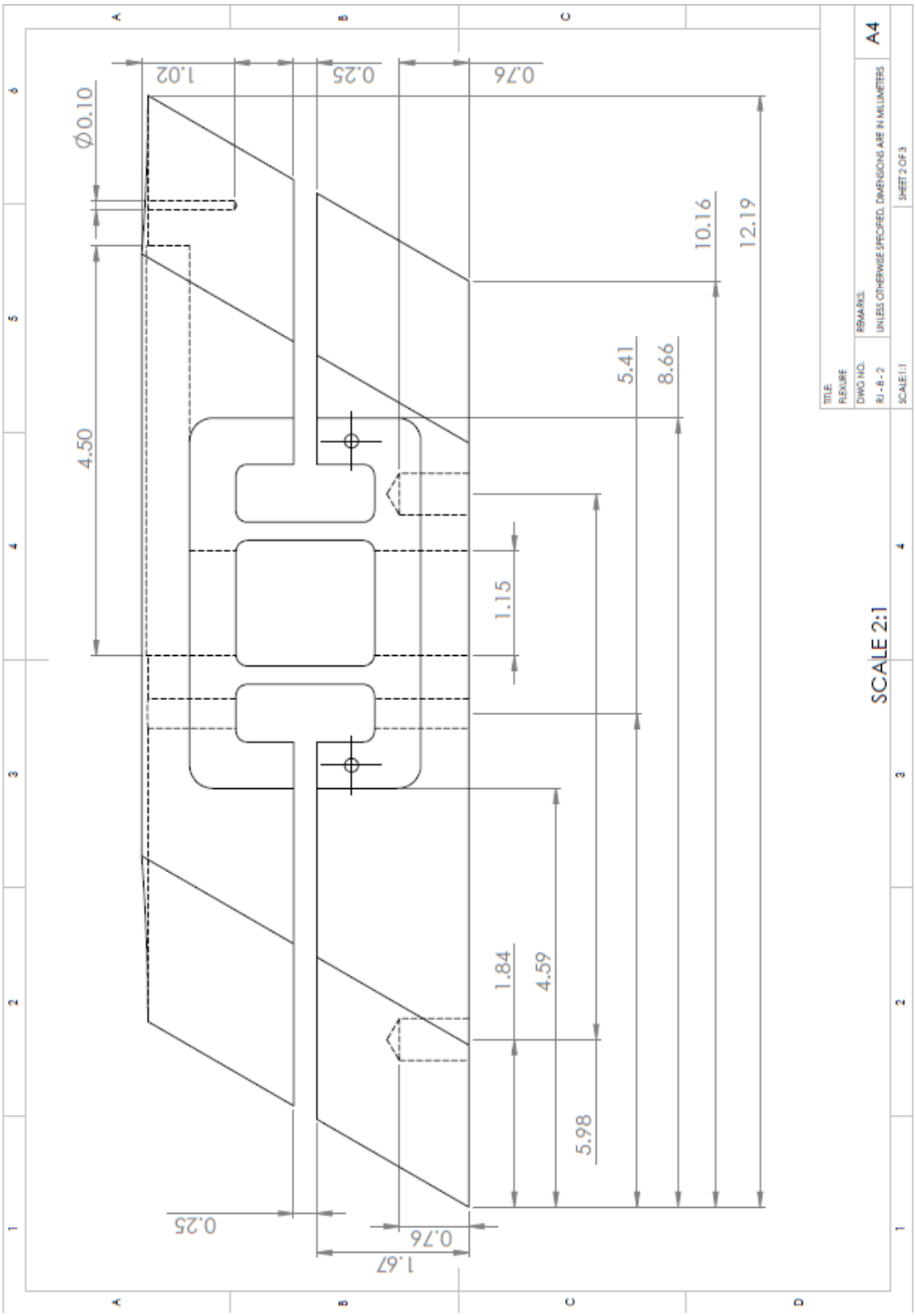

Figure 31 Part drawing: original flexure (RJ – 8 – 2). From [3].

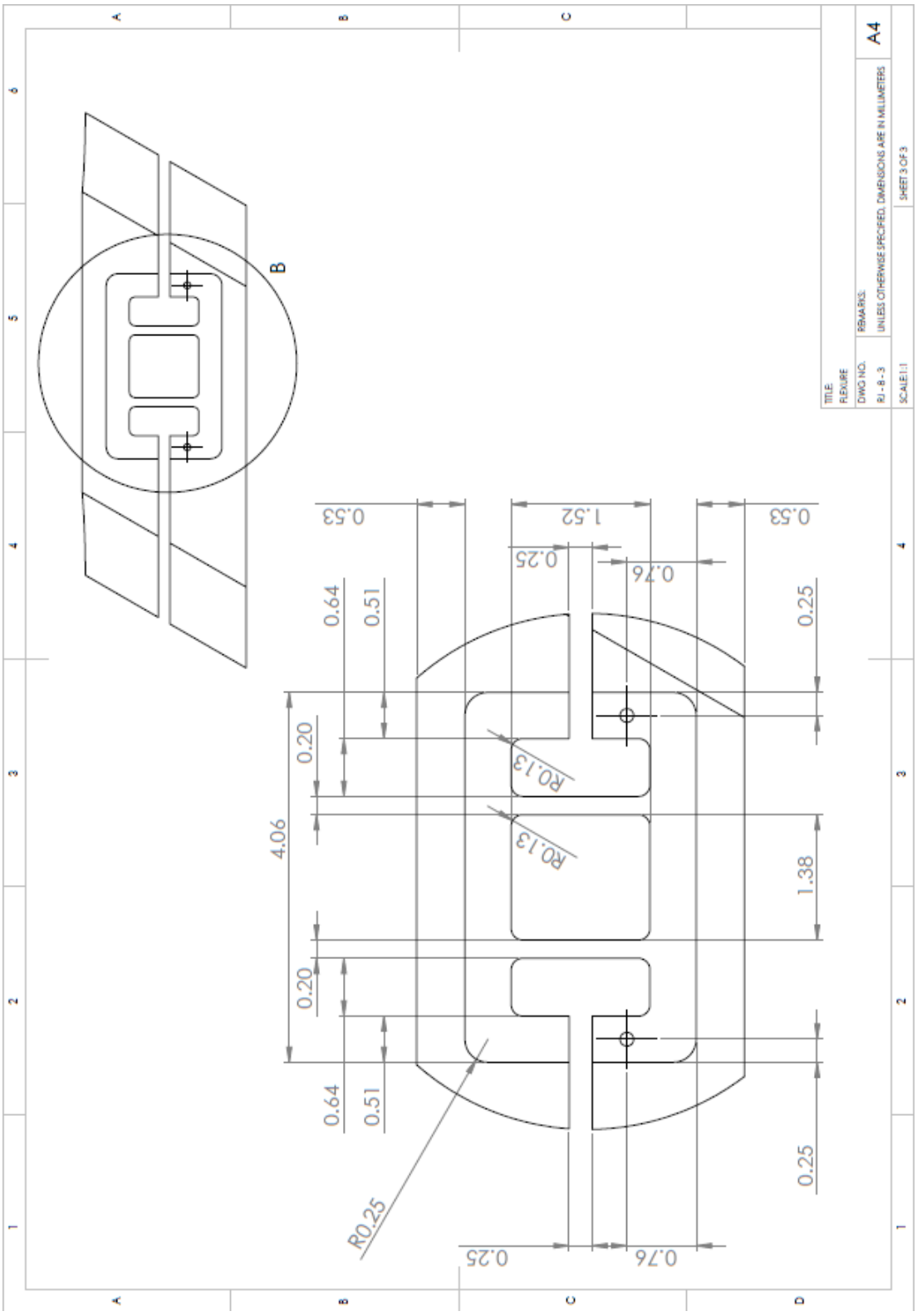

Figure 32 Part drawing: original flexure (RJ – 8 – 3). From [3].

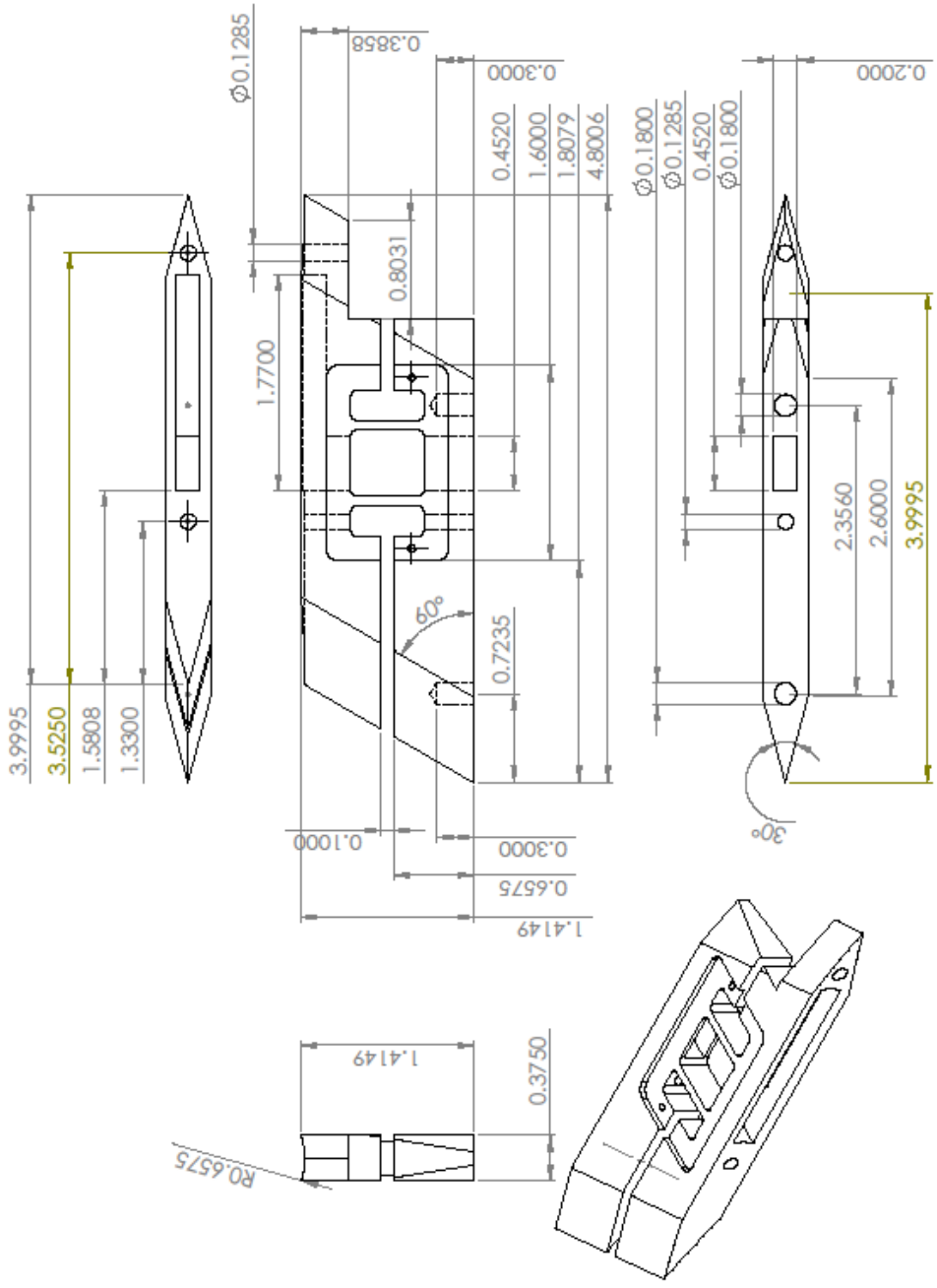

Figure 33 Modified Flexure showing dimensions of the cut made (RJ – 8 – 3). After [3].

THIS PAGE INTENTIONALLY LEFT BLANK

APPENDIX B: EXPERIMENTAL SETUP

A. USER DEFINED INSTRUCTIONS FOR DATA ANALYSIS AND RECORDING WITH NI INSTRUMENTATION

Hardware Setup

- Have NIMAX installed on the computer in use.
- Open NIMAX.
- In command menu, right-click Data Neighborhood and select "create new."
    - Select NI DAQmx Global Virtual Channel
    - Click next
    - Select "Acquire Signals" → "Analog Input" →"Strain"

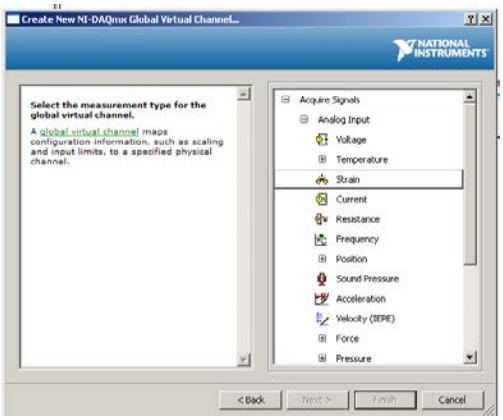

    - Select "ai0," or whichever port will be used on the NI DAQmx
    - Click next,
    - Name the channel "HalfBridge," or whichever name you choose
    - Click finish
- Under Strain Setup, input the relevant data.
    - Max: 1m
    - Min: 1m
    - Gage factor: 2
    - Gage Resistance: 350
    - Initial Voltage: -1.1865m
    - Vex Source: Internal

- Vex Value (V): 2.5
- Strain Configuration: Half Bridge II
- Lead Resistance: 0

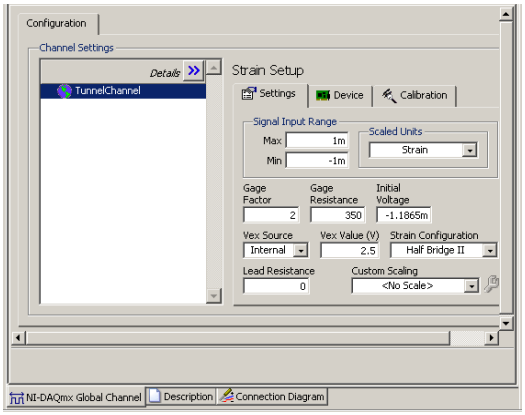

- At bottom, select "connection diagram".
- Reference the diagram in connecting the strain gages to the RJ-50 wire.

  Each strain gage should have one black wire and one white wire connected to it. It does not matter in which order the strain gages are connected, so the arbitrary labels Gage A and Gage B will be used (i.e., either gage can be labeled Gage A, the outcome will be the same).

- Clip off the end of the RJ-50 wire and strip the insulating protection on the wires back ¾ inch.

- Solder the white wire of Gage A together with the black wire of Gage B with the grey RJ-50 wire, which is labeled CH^+ in the diagram.
- Solder the black wire of Gage A with the purple RJ-50 wire, labeled EX^- in the diagram.
- Solder the white wire of Gage B to the blue wire RJ-50 wire, labeled EX^+ on the diagram.

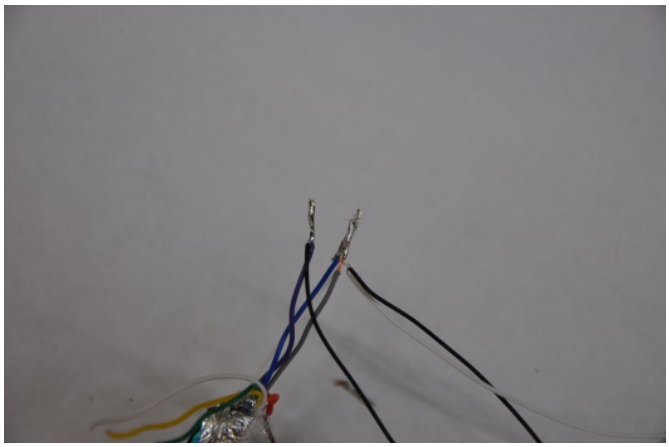

- Shrink wrap the exposed wires.

- Select the Device tab in NIMAX and click “calibrate”.

Uncheck “Enable Shunt Calibration” and click Next.

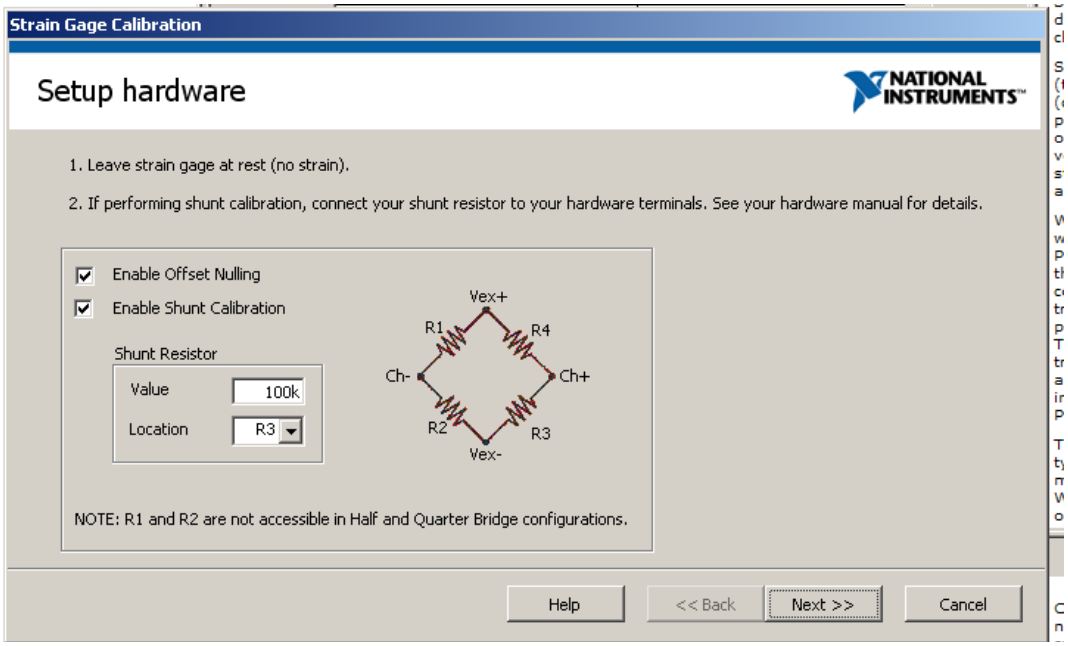

- Click “Measure”.
- After it measures, click “Reset Data”.
- After it resets, click “Calibrate”.
- If it successfully calibrates, click Finish.

- The half bridge can be tested by clicking on the Run button and switching the settings from table to chart. A relatively small force can be applied to the ramjet to test the system. The chart should show a change in the strain readings coinciding to when the force was applied to the ramjet.

Data Collection

- Open NI Max.
- Expand Data Neighborhood.
- Expand NI-DAQmx Global Virtual Channels.
- Pick the channel.

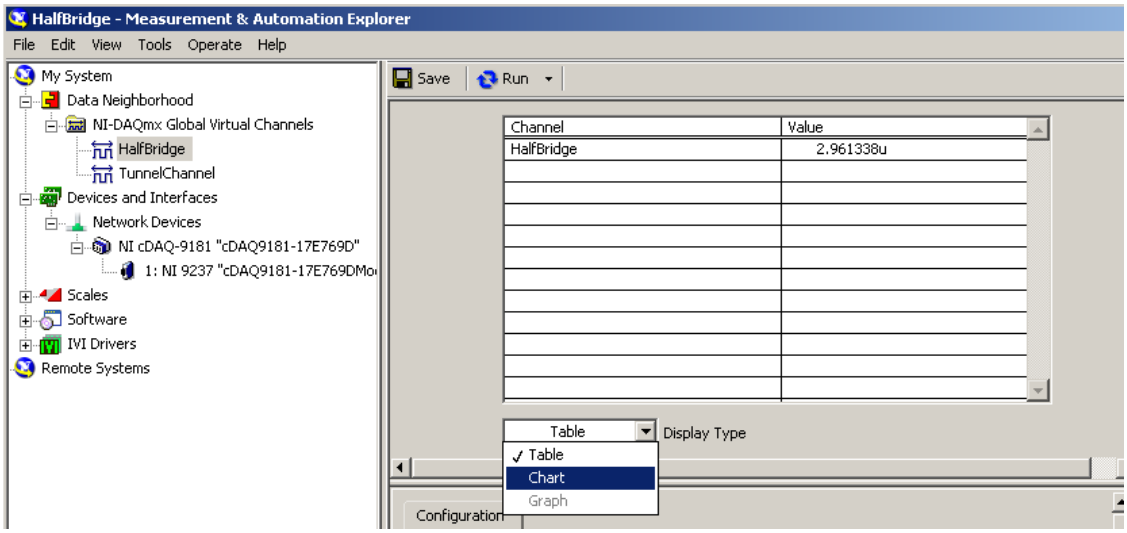

- If the channel is not calibrated, follow the above instructions to calibrate the channel so that the zero is reset. If this is done, the channel should read zero strain for zero load.
- Under the drop down menu for display type, pick chart.
- When data is ready to be collected, click run. NI Max stores 100 sample readings at a time, which correspond to what is shown on the chart at any given moment.
- When the data of interest is collected and on display on the chart, click stop.
- mouse over the top right corner of the chart and right click on the squiggly blue line that pops up. Choose export >> export data to excel.

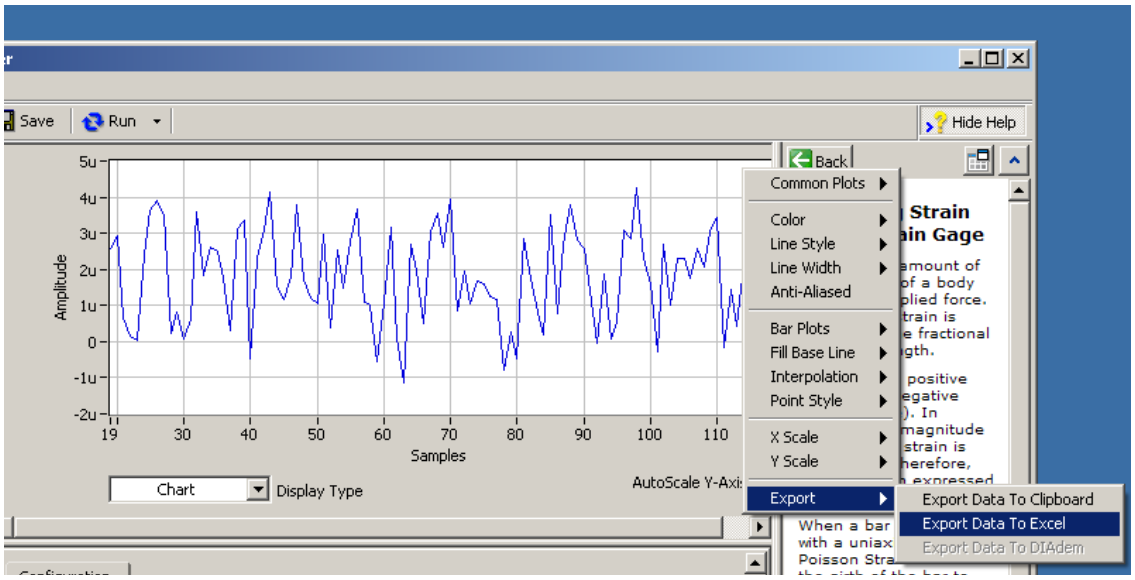

- Save the excel file to a document folder.

The above procedure can be repeated any number of times without shutting down NI Max.

"DAQ Assistant Error" Correction

- When NI Max is open, expand Devices and Interfaces.
- Expand Network Devices.
- click on NI cDAQ-9181.

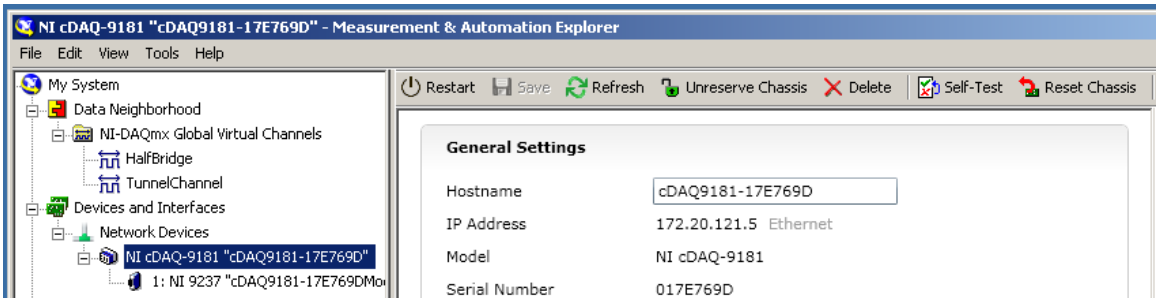

- click self test

THIS PAGE INTENTIONALLY LEFT BLANK

APPENDIX C: RESULTS FROM SSWT EXPERIMENTATION

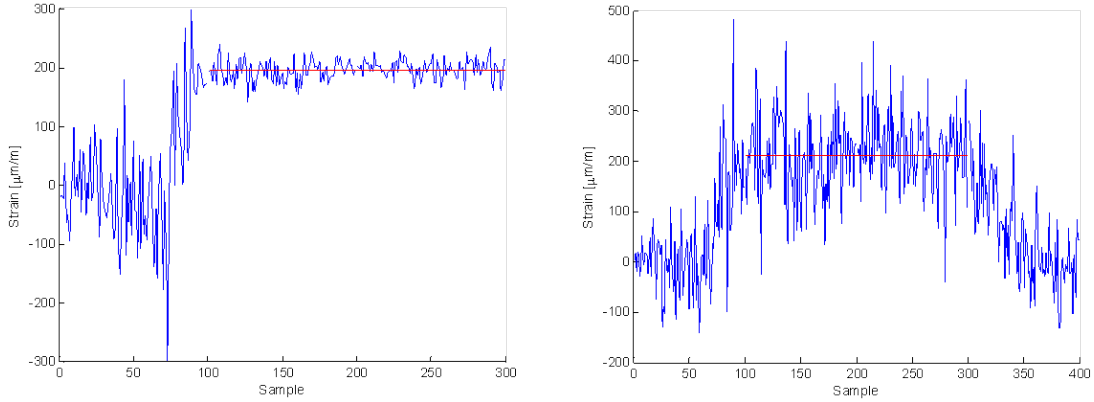

Figure 34 Results from SSWT run on 12 February 2013 with nozzle A.

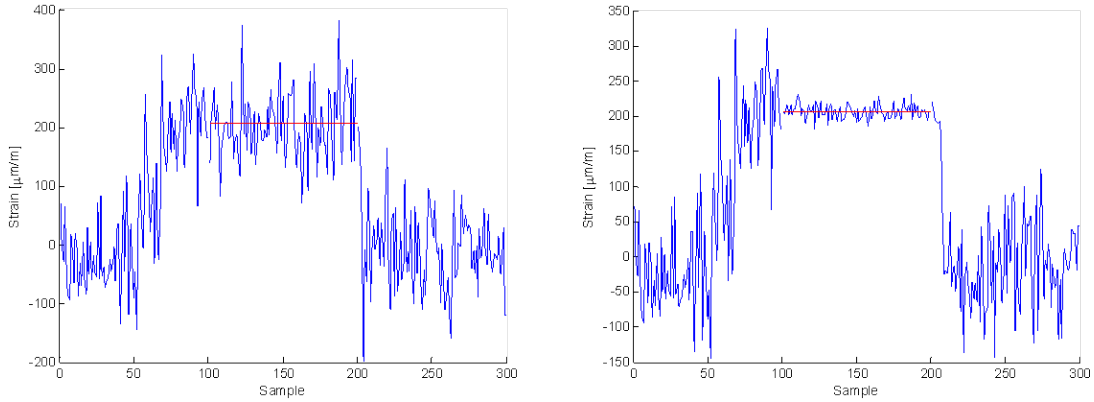

Figure 35 Results from SSWT run on 30 April 2013 with Nozzle A.

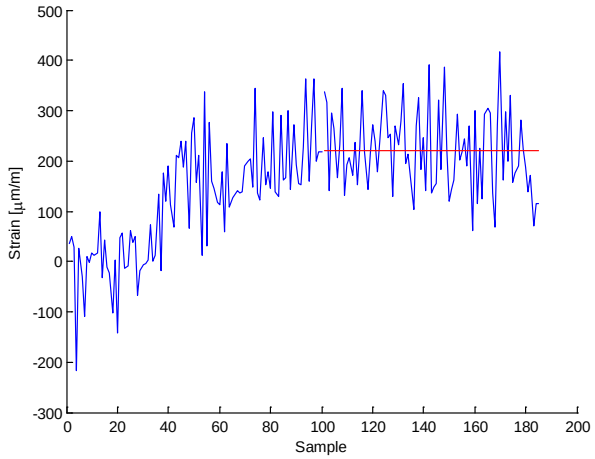

Figure 36 Results from SSWT run on 12 June 2013 with Nozzle B.

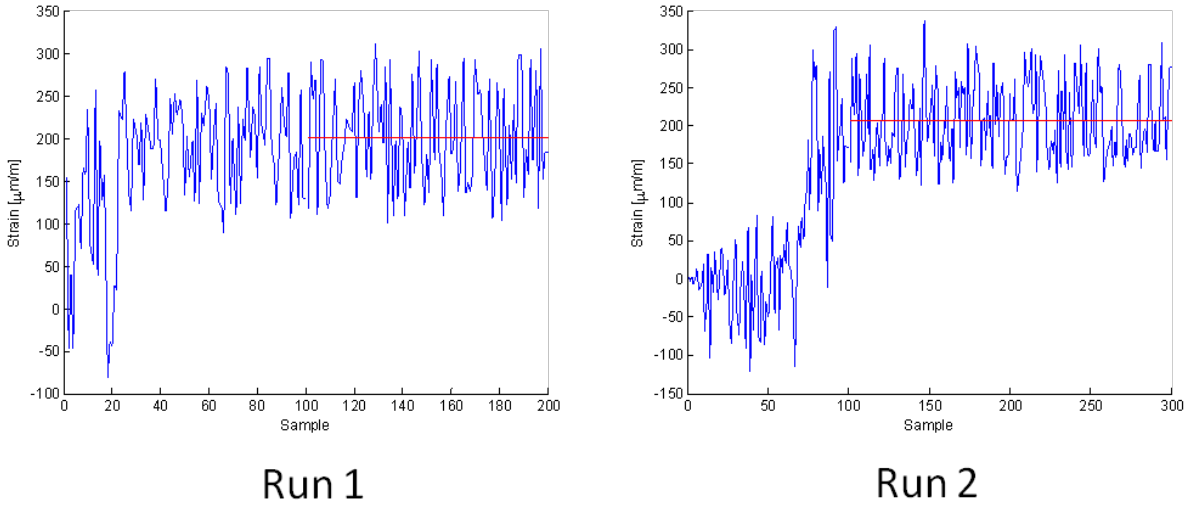

Figure 37 Results From SSWT run on 13 June 2013 with Nozzle C.

APPENDIX D: COLD FLOW COMPUTATIONAL SETUP

A. MESH SETUP

The mesh setup for this cold flow simulation has the same parameters as those listed in Appendix A1 of [3]. However the inflation layers are altered slightly. The following tables have been taken from [3] and have been modified to show the parameters of this cold flow setup.

Scope	
Scoping Method	Geometry Selection
Geometry	1 body
Definition	
Suppressed	No
Boundary Scoping Method	Named Selections
Boundary	Ramjet
Inflation Option	Total Thickness
- Number of Layers	20
- Growth Rate	1.05
- Maximum Thickness	1e-4m
Inflation Algorithm	Pre

Table 6 Inflation settings for Ramjet boundary. After [3].

Scope	
Scoping Method	Geometry Selection
Geometry	1 body
Definition	
Suppressed	No
Boundary Scoping Method	Named Selections
Boundary	Winglet
Inflation Option	Total Thickness
- Number of Layers	20
- Growth Rate	1.05
- Maximum Thickness	1e-4m
Inflation Algorithm	Pre

Table 7 Inflation settings for Winglet boundary. After [3].

B. CFX-PRE SETUP

The parameter setup for this cold flow analysis is the same as the setup delineated in Appendix A2 of [3] for the Default Domain, Expert Parameters, Convergence Control, and the Inlet, Outlet, Symmetry, and Ramjet boundary conditions. The conditions for the Sides and Winglet in this cold flow analysis are the same as the conditions for the Top and Ramjet boundaries respectively in Appendix A2 of [3]. Figures 38 - 43 show the boundaries for this cold flow analysis.

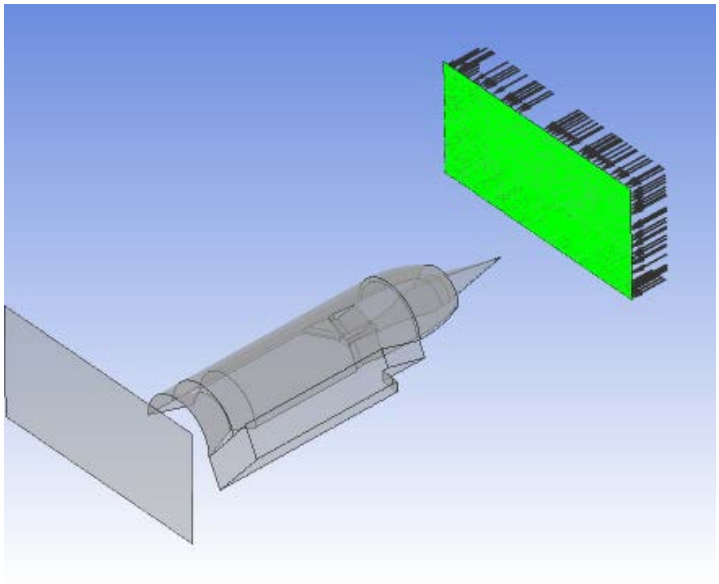

Figure 38 Inlet boundary.

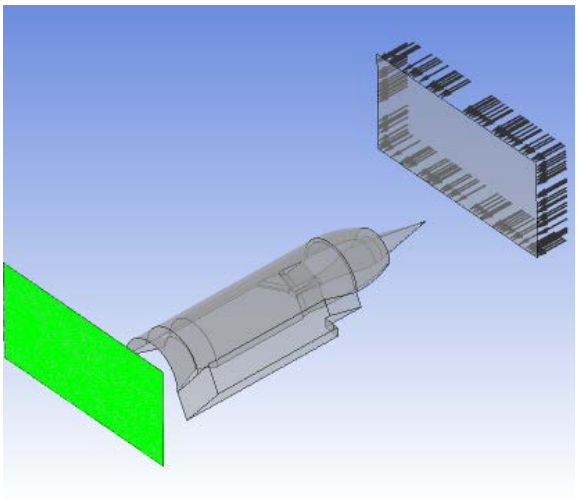

Figure 39 Outlet boundary.

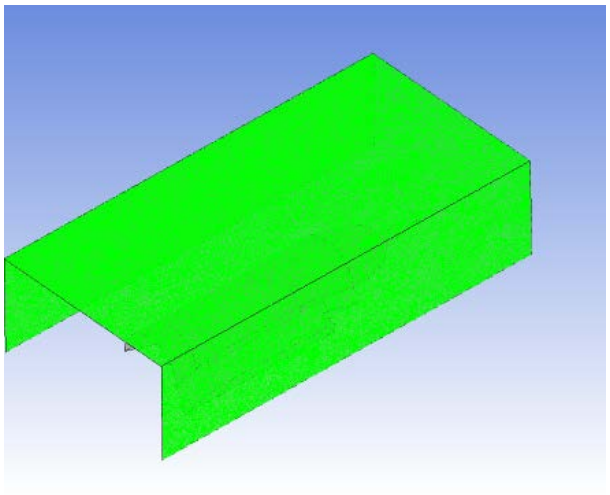

Figure 41 Sides boundary conditions.

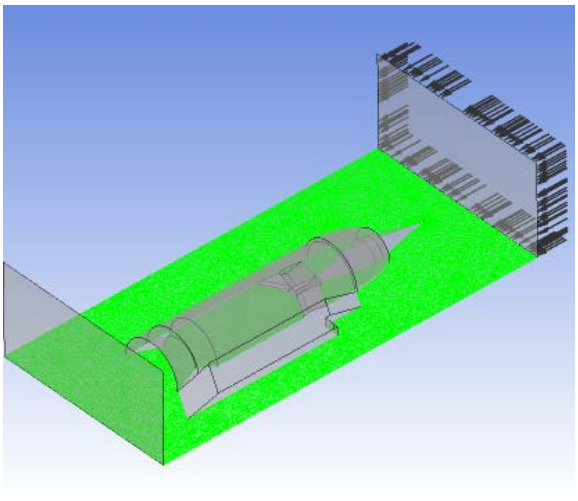

Figure 40 Symmetry boundary.

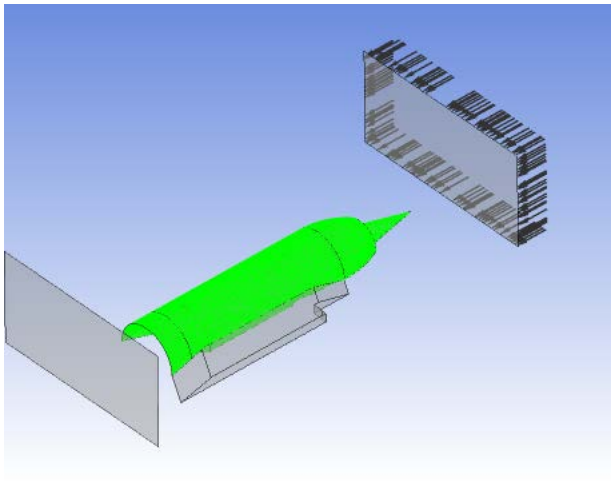

Figure 42 Ramjet boundary.

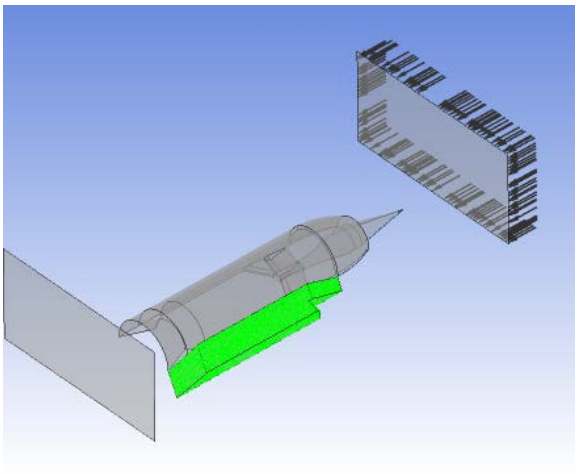

Figure 43 Winglet boundary.

APPENDIX E: COMBUSTION VALIDATION SETUP

The following tables and figures show the setup for the combustion validation test that was run on ANSYS-CFX. The computational model can be repeated by using a geometry file like SolidWorks of the combustor dimensions listed in [4] and setting the ANSYS-Pre parameters to those in the table below. All Tables are after [3].

A. MESH SETTINGS

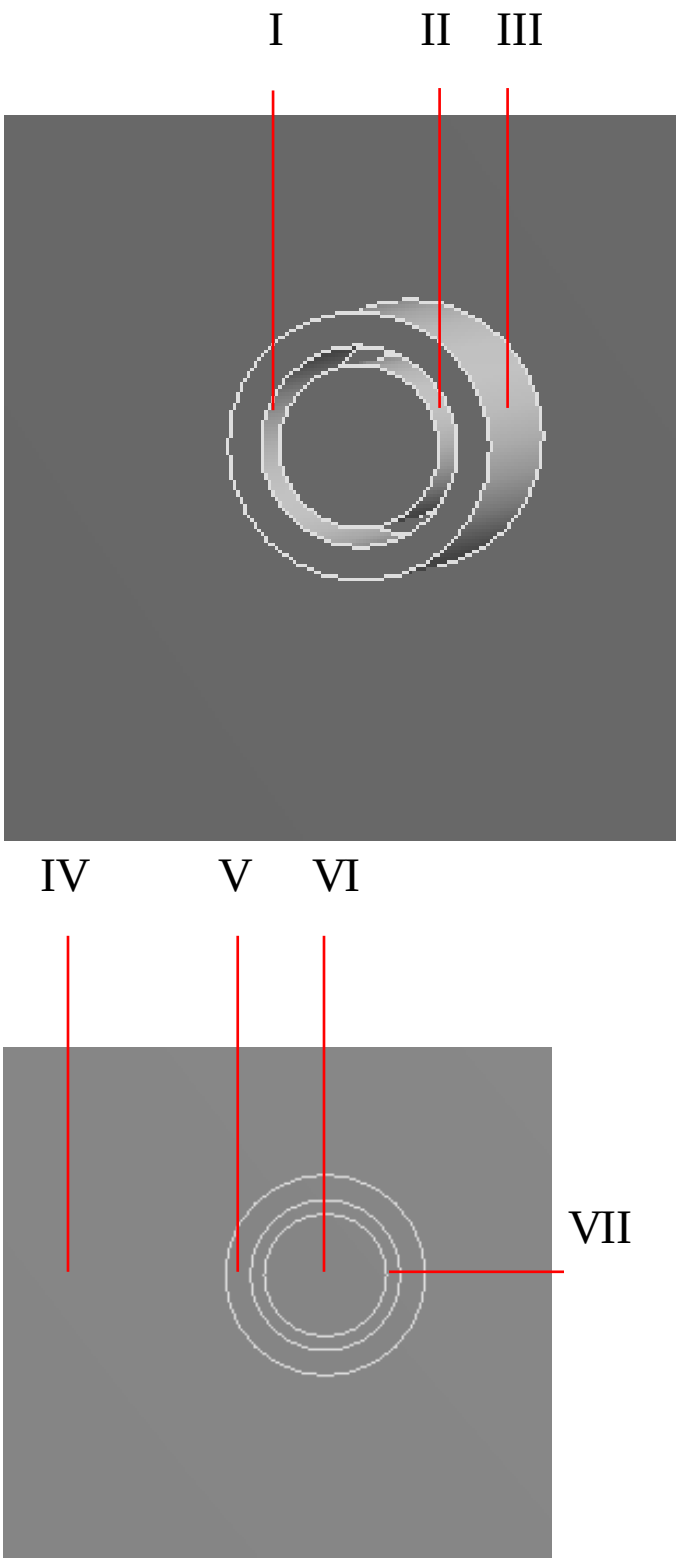

Figure 44 Combustor inlet surfaces.

Defaults	
Physics Preference	CFD
Solver Preference	CFX
Relevance	0
Sizing	
Use Advance Size Function	On: Proximity and Curvature
Relevance Centre	Fine
Initial Size Seed	Active Assembly
Smoothing	Medium
Transition	Slow
Span Angle Centre	Fine
- Curvature Normal Angle	8 deg
- Proximity Accuracy	0.5
- Num Cells Across Gap	Default (3)
- Min Size	0.0005 m
- Proximity Min Size	Default
- Max Face Size	0.001 m
- Max Size	0.001 m
- Growth Rate	1.10
Inflation	
Use Automatic Inflation	None
Patch Conforming Option	
Triangle Surface Mesher	Program Controlled
Advance	
Shape Checking	CFD
Element Midside Nodes	Dropped
Extra Retries for Assembly	Yes
Mesh Morphing	Disabled

Table 8 Mesh Settings

Scope	
Scoping Method	Geometry Selection
Boundary (Face)	VI
Definition	
Suppressed	No
Type	Element Size
- Element Size	5.e-004 m
Behavior	Soft
- Curvature Normal Angle	Default
- Growth Rate	Default

Table 9 Face sizing 1 settings

Scope	
Scoping Method	Geometry Selection
Boundary (Faces)	IV, VII
Definition	
Suppressed	No
Type	Element Size
- Element Size	1.e-004 m
Behavior	Soft
- Curvature Normal Angle	Default
- Growth Rate	Default

Table 10 Face sizing 2 settings

Scope	
Scoping Method	Geometry Selection
Geometry	The entire domain
Definition	
Suppressed	No
Boundary Scoping Method	Geometry Selection
Boundary (Faces)	I, II, III, IV, VII
Inflation Option	Total Thickness
- Number of Layers	9
- Growth Rate	1.2
- Maximum Thickness	5.e-004m
Inflation Algorithm	Pre

Table 11 Inflation layer settings

B. CFX PRE SETUP

BASIC SETTINGS	
Location and Type - Location - Domain Type - Coordinate Frame	 <use default> Fluid Domain Coord 0
Fluid and Particles Definition for Fluid 1 - Option: - Material - Morphology	 Material Library Gas Phase Combustion: Hydrogen Oxygen Continuous Fluid
Domain Models - Pressure → Reference Pressure - Buoyancy Model → Option - Domain Motion → Option - Mesh Deformation → Option	 1.18 [MPa] Non-Buoyant Stationary None
FLUID MODELS	
Heat Transfer → Option Incl. Viscous Dissipation	Total Energy Checked
Turbulence - Option - Transitional Turbulence - Turbulent Flux Closure for Heat Transfer - Option	 Shear Stress Transport Gamma Theta Model Checked Eddy Diffusivity
Combustion → Option **Maximum Flame Temperature** - Maximum Flame Temperature	Eddy Dissipation Checked 3473 [K]
Thermal Radiation → Option	None
H2, H2O, O2 **N2**	Option: Transport Equation Option: Constraint

Table 12 Default domain setup

BASIC SETTINGS	
Boundary Type	Inlet
Location	VI
BOUNDARY DETAILS	
Flow Regime → Option	Subsonic
Mass and Momentum	
- Option	Mass Flow Rate
- Rel. Static Pressure	0.042 [kg s^-1]
Turbulence → Option	Intensity Length Scale
- Fractional Intensity	0.2
- Eddy Length Scale	0.02 [m]
Heat Transfer	
- Option	Static Temperature
- Static Temperature	300 [K]
H2 Mass Fraction	0
O2 Mass Fraction	0.99
H2O Mass Fraction	0.001

Table 13 Oxygen inlet settings

BASIC SETTINGS	
Boundary Type	Inlet
Location	V
BOUNDARY DETAILS	
Flow Regime → Option	Subsonic
Mass and Momentum - Option - Rel. Static Pressure	 Mass Flow Rate 0.0103 [kg s^-1]
Turbulence → Option - Fractional Intensity - Eddy Length Scale	Intensity Length Scale 0.2 0.02 [m]
Heat Transfer - Option - Static Temperature	 Static Temperature 300 [K]
H2 Mass Fraction O2 Mass Fraction H2O Mass Fraction	1 0 0

Table 14 Hydrogen inlet settings

BASIC SETTINGS	
Boundary Type	Outlet
Location	Outlet
BOUNDARY DETAILS	
Flow Regime → Option	Subsonic
Mass And Momentum→ Option Relative Pressure Pres. Profile Blend	Average Static Pressure 0 [atm] 0.05
Pressure Averaging→ Option	Average Over Whole Outlet

Table 15 Outlet settings

BASIC SETTINGS	
Boundary Type	Wall
Location	Walls
BOUNDARY DETAILS	
Mass and Momentum → Option	No Slip Wall
Wall Roughness → Option	Smooth Wall
Heat Transfer → Option	Adiabatic

Table 16 Wall settings

BASIC SETTINGS	
Advection Scheme --> Option	High Resolution
Turbulence Numerics --> Option	First Order
Convergence Control	
- Min. Iterations	1
- Max. Iterations	100
- Fluid Timescale Control	
+ Timescale Control	Auto Timescale
+ Length Scale Option	Conservative
+ Timescale Factor	1.0
Convergence Criteria	
- Residual Type	RMS
- Residual Target	1.00E-04
ADVANCE OPTIONS	
Global Dynamic Model Control	Checked

Table 17 Solver control settings

THIS PAGE INTENTIONALLY LEFT BLANK

APPENDIX F: RAMJET COMBUSTION SETUP

A. MESH SETUP

The Mesh parameters are set after setting up the computational domain. The domain was defined using SolidWorks models of both the ramjet and a block that represented the air the ramjet was situated in. Once the computational domain is defined, the meshing parameters are those defined in Appendix A, section A1 of [3].

B. CFX PRE SETUP

BASIC SETTINGS	
Location and Type - Location - Domain Type - Coordinate Frame	 <use default> Fluid Domain Coord 0
Fluid and Particles Definition for Fluid 1 - Option: - Material - Morphology	 Material Library Gas Phase Combustion: Hydrogen Oxygen Continuous Fluid
Domain Models - Pressure → Reference Pressure - Buoyancy Model → Option - Domain Motion → Option - Mesh Deformation → Option	 0 [Pa] Non-Buoyant Stationary None
FLUID MODELS	
Heat Transfer → Option Incl. Viscous Dissipation	Total Energy Checked
Turbulence - Option - Transitional Turbulence	 Shear Stress Transport Gamma Theta Model
Combustion → Option - Chemical Timescale	Eddy Dissipation 0.0001 [s]
Thermal Radiation → Option	None
H2, H2O, O2 **N2**	Option: Transport Equation Option: Constraint

Table 18 Default domain setup

BASIC SETTINGS	
Boundary Type	Inlet
Location (face)	Inlet
BOUNDARY DETAILS	
Flow Regime → Option	Supersonic
Mass and Momentum	
- Option	Normal Speed & Pressure
- Rel. Static Pressure	101325 Pa
- Normal Speed	1369.9 m/s
Turbulence → Option	High (Intensity = 10%)
Heat Transfer	
- Option	Static Temperature
- Static Temperature	292K
H2 Mass Fraction	0.0
H2O Mass Fraction	0.005
O2 Mass Fraction	0.232

Table 19 Air inlet settings

BASIC SETTINGS	
Boundary Type	Inlet
Location	Injection Ports
BOUNDARY DETAILS	
Flow Regime → Option	Subsonic
Mass and Momentum	
- Option	Normal Speed
- Rel. Static Pressure	75 [m s^-1]
Turbulence → Option	Intensity Length Scale
- Fractional Intensity	0.2
- Eddy Length Scale	0.02 [m]
Heat Transfer	
- Option	Static Temperature
- Static Temperature	300 [K]
H2 Mass Fraction	1
O2 Mass Fraction	0.0
H2O Mass Fraction	0.0

Table 20 Injection port inlet settings

BASIC SETTINGS	
Boundary Type	Outlet
Location	Outlet
BOUNDARY DETAILS	
Flow Regime → Option	Supersonic

Table 21 Outlet settings

BASIC SETTINGS	
Boundary Type	Wall
Location	Walls

Table 22 Wall settings

BASIC SETTINGS	
Advection Scheme --> Option	High Resolution
Turbulence Numerics --> Option	High Resolution
Convergence Control	
- Min. Iterations	1
- Max. Iterations	150
- Fluid Timescale Control	
+ Timescale Control	Auto Timescale
+ Length Scale Option	Conservative
+ Timescale Factor	1.0
Convergence Criteria	
- Residual Type	RMS
- Residual Target	1.00E-06
ADVANCE OPTIONS	
Global Dynamic Model Control	Checked
Temperature Damping > option	Automatic
Compressibility Control > High Speed Numerics	checked

Table 23 Solver control settings

Linear Solver	
Solver Relaxation Fluids	0.9
Solver Relaxation Scalar	0.9
Convergence Control	
Memory Control	
Topology estimate factor	1.2
High Speed Models	
Max continuity loops > Value	3

Table 24 Expert parameters settings

LIST OF REFERENCES

[1] K. M. Ferguson, "Design and cold flow evaluation of a miniature Mach 4 ramjet," M.S. Thesis, Department of Aeronautical Engineering., Naval Postgraduate School, Monterey, CA, June 2003.

[2] W. T. Khoo, "Cold flow drag measrement and nmerical performance prediction of a miniature ramjet at Mach 4," M.S. Thesis, Department of Aeronautical Engineering, Naval Postgraduate School, Monterey, CA, December 2003.

[3] B. Chen, "Numerical performance prediction of a miniature ramjet at Mach 4," M.S. Thesis, Department of Mechanical and Aerospace Engineering, Naval Postgraduate School, Monterey, CA, September 2012.

[4] M.J. Foust et al., "Experimental and analytical characterization of a shear coaxial combusting GO2/GH2 flowfield," presented at the American Institute of Aeronautics and Astronautics 34th Aerospace Sciences Meeting and Exhibit, Reno, NV, January 15–18, 1996, Paper 96-0646.

THIS PAGE INTENTIONALLY LEFT BLANK

INITIAL DISTRIBUTION LIST

1. Defense Technical Information Center
   Ft. Belvoir, Virginia

2. Dudley Knox Library
   Naval Postgraduate School
   Monterey, California